Journal of Computational Neuroscience (2019) 46:211–232
https://doi.org/10.1007/s10827-019-00712-w

A coarse-graining framework for spiking neuronal networks: from strongly-coupled conductance-based integrate-and-fire neurons to augmented systems of ODEs

Jiwei Zhang[1,2] · Yuxiu Shao[3,4] · Aaditya V. Rangan[5] · Louis Tao[3,4]

Received: 5 August 2018 / Revised: 27 January 2019 / Accepted: 31 January 2019 / Published online: 16 February 2019

Abstract

Homogeneously structured, fluctuation-driven networks of spiking neurons can exhibit a wide variety of dynamical behaviors, ranging from homogeneity to synchrony. We extend our partitioned-ensemble average (PEA) formalism proposed in Zhang et al. (*Journal of Computational Neuroscience, 37*(1), 81–104, 2014a) to systematically coarse grain the heterogeneous dynamics of strongly coupled, conductance-based integrate-and-fire neuronal networks. The population dynamics models derived here successfully capture the so-called multiple-firing events (MFEs), which emerge naturally in fluctuation-driven networks of strongly coupled neurons. Although these MFEs likely play a crucial role in the generation of the neuronal avalanches observed *in vitro* and *in vivo*, the mechanisms underlying these MFEs cannot easily be understood using standard population dynamic models. Using our PEA formalism, we systematically generate a sequence of model reductions, going from Master equations, to Fokker-Planck equations, and finally, to an augmented system of ordinary differential equations. Furthermore, we show that these reductions can faithfully describe the heterogeneous dynamic regimes underlying the generation of MFEs in strongly coupled conductance-based integrate-and-fire neuronal networks.

Keywords Spiking neurons · Synchrony · Homogeneity · Multiple firing events · Partitioned-ensemble-average · Maximum entropy principle · Coarse-graining method

1 Author summary

Through a carefully designed ensemble average (Zhang et al. 2014a), we constructed a coarse-graining formalism that was used to study the heterogeneous dynamics of current-based integrate-and-fire neuronal networks. In Zhang and Rangan (2015), we showed that this reduction is capable of capturing the dynamical emergence of multiple-firing events (MFEs) that may underlie the neuronal avalanches observed *in vitro* and *in vivo*. Here we extend this formalism to coarse grain the heterogeneous dynamics of strongly coupled conductance-based integrate-and-fire neuronal networks. Our systematic reduction, from first principles, offers analytically tractable population dynamic models, which are not only capable of faithfully reproducing network dynamics ranging from homogeneity to MFEs, but also provides a conceptually intuitive framework to dramatically reduce and capture the effective dimensions of the emergent dynamics of strongly coupled neuronal networks.

Action Editor: Alain Destexhe

✉ Louis Tao
taolt@mail.cbi.pku.edu.cn

Extended author information available on the last page of the article.

2 Introduction

Strongly coupled networks in the brain often exhibit a rich repertoire of dynamics, ranging from homogeneity to synchrony, reflecting the many possible interactions between excitation and inhibition, between multiple synaptic timescales, and between short-range and long-range recurrent connections. The heterogeneous dynamics observed in various brain regions (e.g., mammalian motor and visual cortex, rat auditory cortex and mammalian hippocampus among others Kenet et al. 2003; Hatsopoulos et al. 1998; Csicsvari et al. 2000; Leinekugel et al. 2002; Samonds et al. 2005; Mazzoni et al. 2007; Sakata and Harris 2009; Petermann et al. 2009; Churchland et al. 2010; Yu and Ferster 2010; Hahn et al. 2010; Plenz et al. 2011; Shew et al. 2011; Dehghani

et al. 2012; Yu et al. 2011) often involve collective population responses, which can be very sensitive to both external inputs and the internal state of the network (Traub et al. 1999; Bruzsaki and Draguhn 2004; Seejnowski and Paulsen 2006; Roopum et al. 2008; Fries 2009). Furthermore, the emergent collective dynamics is believed to be significant contributor to information coding and other essential brain functions (Singer 1999).

Recent experimental and simulational studies have shown the prevalence of strong self-organized, synchronous network activity in the form of multiple firing events (MFEs) (Yu et al. 2011; Rangan and Young 2013b; Hansel and Sompolinsky 1996; Kriener et al. 2008; Rangan and Young 2013a), i.e., the almost synchronous spiking activity of variable temporal duration and variable population sizes. The main mechanism underlying this type of emergent heterogeneous dynamics appears to be the strong competition between excitatory and inhibitory subpopulations. Much theoretical work have focused on analyzing the dynamical effects of structured architecture and correlated inputs (Vogels and Abbott 2005; Rangan 2009; Zhao et al. 2011; Hu et al. 2013), while others have focused on investigating the emergent dynamics of a network state of high gain (Brunel 2000; Buice and Chow 2007; Cardanobile and Rotter 2010; Battaglia and Hansel 2011).

One of major challenges in theoretical neuroscience is to develop methods from first principles to systematically coarse grain the emergent network dynamics. Standard population dynamics techniques cannot easily describe the full range of complex dynamics ranging from homogeneity to synchrony to MFEs. In Zhang et al. (2014a), we carefully designed a specific ensemble average, a 'partitioned ensemble average' (PEA), by introducing, at each time step, a transition rate from the nucleation to the release of an MFE that can be evaluated efficiently. This PEA framework has faithfully captured a broad range of dynamic regimes observed in simulations of current-based integrate-and-fire (IF) neuronal networks (Zhang et al. 2014a; Zhang and Rangan 2015).

In this paper we will extend the PEA framework to study the heterogeneous dynamics of the conductance-based IF neuronal networks. Conductance-based IF neurons are more realistic models of spiking neurons (Koch 1999), as synaptic conductances introduce dynamical time-scales that are unaccounted for in the current-based models. Typically, *in vivo*, individual neurons in active networks receive total synaptic conductances that are larger than their leak conductances (Destexhe and Pare 1999). These so-called high conductance states are thought to endow the network with certain computational advantages, e.g., enhanced responsiveness (Destexhe et al. 2003; Richardson 1918) and sharper temporal processing (Destexhe et al. 2003; Shelley et al. 2002). To capture the essential dynamical features of MFEs, the idea behind the PEA framework arose from the observations of MFE dynamics in neuronal network simulations, where the typical de-correlation time-scale of network neurons is much shorter than the inter-MFE intervals. Therefore, we construct the PEA framework to solve population dynamics models *conditioned* on the probability of occurrence of an MFE at each time step. The transition rate (i.e., the probability of occurrence of an MFE) can be calculated by using the current state of the population dynamics model. Whenever an MFE occurs, we pause the population dynamics model, and compute an MFE from the synaptic coupling strengths and voltage distributions of the network at this time. Then, we use the voltage distribution of the network immediately after the MFE as the initial condition for further numerical evolution of the population dynamics model. As we shall see below, a number of population models can be used, each with its own advantages and applications.

Our PEA allows us to derive a coarse-grained reduction of conductance-based IF neuronal network directly from first principles. From a Master equation description, we derive the corresponding Fokker-Planck (FP) system. We further reduce the system by introducing voltage moments, leading to a hierarchy of moments, which can then be closed using the maximum entropy principle, and finally resulting in an augmented system of ODEs. This profound reduction is not only successful at simulating homogeneous and synchronous network activity but can also faithfully capture highly heterogenous neuronal network dynamics such as the MFEs. Furthermore, it also provides a conceptual framework to dramatically reduce the effective dimensions of the neuronal network dynamics.

The outline of this paper is as follows. In Section 3, we introduce the conductance-based IF neuronal network, and briefly discuss the underlying spiking network dynamics, as well as some of the pertinent features of MFEs. In Section 4, we review the basic framework of our PEA, focusing on how we can design it to use standard population models to capture MFEs. In Section 5, we derive a reduction of spiking neuronal network dynamics from the standard Master equation, to a Fokker-Planck equation and finally, to an augmented system of ODEs via the maximum entropy principle. In Section 6, we give numerical examples to illustrate the capability and effectiveness of our approach at capturing the dynamical features of MFEs. We end this paper with concluding remarks and a discussion of future work.

3 Multiple firing events in IF networks

In this section, we introduce the conductance-based IF neuronal network, describe the underlying spiking

population dynamics, present a method to resolve MFEs when the synapses are infinitely fast, and investigate the influence of conductance-based synaptic connections on the network voltage distribution, firing rates, and other emergent statistical features of MFEs.

3.1 Integrate-and-fire network model

To exclude any effects of network-connectivity fluctuations arising from heterogeneous couplings, we consider the following all-to-all coupled network of N_E excitatory neurons and N_I inhibitory neurons, with the i^{th} neuron's membrane potential evolving according to

$$\frac{dV_i^Q}{dt} = -g_L\left(V_i^Q - V_L\right) - g^E\left(V_i^Q - V_E\right) - g^I\left(V_i^Q - V_I\right), \quad (1)$$

$$\tau_E \frac{dg^E}{dt} = -g^E + \sum_{\ell} S^{QY}\delta\left(t - t_{i\ell}^Q\right) + \sum_{j,k} S^{QE}\delta\left(t - t_{jk}^E\right), \quad (2)$$

$$\tau_I \frac{dg^I}{dt} = -g^I + \sum_{j,k} S^{QI}\delta\left(t - t_{jk}^I\right), \quad (3)$$

for $i = 1, \cdots, N_Q$, where $Q \in \{E, I\}$ labels excitatory and inhibitory. The membrane potential of the neuron is $V^Q(t) = V_{\text{in}} - V_{\text{out}}$, where V_{in} is the intracellular voltage and V_{out} is the extracellular voltage. We use the difference between the spike threshold and reset to non-dimensionalize the membrane potential and set $V_T = 1$, $V_L = V_R = 0$. Then the excitatory and inhibitory reversal potentials become $V_E = 14/3$ and $V_I = -2/3$. In these reduced dimensional units, the leak conductance is $g_L = 0.05$/ms (see Cai et al. 2004). In integrate-and fire dynamics, whenever the voltage V_i^Q reaches a threshold V_T, a spike has occurred and is recorded with a spike time t_{ik}^Q, where the subscript ik represents the k-th spike of the i-th neuron. The membrane potential V_i^Q is then reset to V_R. Furthermore, when a Q'-type neuron fires, it creates an instantaneous jump in the conductance of the Q-type postsynaptic neuron with coupling strength $S^{QQ'}$ with $Q, Q' \in \{E, I\}$. For external input, the spike-time $t_{i\ell}^Q$ models the ℓ-th spike for excitatory conductance of the ith Q-type neuron with an independent realization of the Poisson process with rate m_{net}^{QY} and strength S^{QY}.

To determine whether or not a single neuron's spiking has induced another neuron to fire, we assume that the synaptic time courses are very fast, that is, much shorter than the membrane time constant. In this situation, we consider the limit of 'infinitely-fast conductances', i.e., the limit where $\tau_E \to 0$ and $\tau_I \to 0$. This has the effect that one excitatory neuron firing will make another Q-type neuron's voltage v jump immediately by

$$R\left(v, S^{QE}\right) = V_E + (v - V_E)\, e^{-S^{QE}}. \quad (4)$$

Similarly, one external Poisson input spike, and one inhibitory neuron firing will make a Q-type neuron's voltage jump, respectively, by

$$R\left(v, S^{QY}\right) = V_E + (v - V_E)\, e^{-S^{QY}},$$
$$\text{and } R\left(v, S^{QI}\right) = V_I + (v - V_I)\, e^{-S^{EE}}. \quad (5)$$

The inverses of the jump R are given by

$$T\left(v, S^{QQ'}\right) = V_E + (v - V_E)\, e^{S^{QQ'}},$$
$$\text{and } T\left(v, S^{QI}\right) = V_I + (v - V_I)\, e^{S^{QI}} \quad (6)$$

with $Q' \in \{Y, E\}$. The derivations of $T(v, S^{QQ'})$ and $R\left(v, S^{QE}\right)$ are detailed in Cai et al. (2006) and Nykamp (2000).

Network Parameters and Notations Our goal in this paper is to develop an analytical framework which connects the 10-dimensional parameters of the IF-network to the network's emergent behavior. The 10-dimensional network parameters are given by

1. Network size: N_I and N_E;
2. External input rates: m_{net}^{IY}, m_{net}^{EY}; and strengths S^{IY}, S^{EY};
3. Synaptic coupling strengths: S^{II}, S^{IE}, S^{EI}, S^{EE}.

In the examples studied in this paper, most of these parameters are bounded by physiological limitations (see Zhang and Rangan 2015; Kohn and Smith 2005; Grill-Spector and Weiner 2014; Stern et al. 1997; Anderson et al. 2000).

We introduce a Klimontovich distribution to describe the voltage configurations $\boldsymbol{\varrho}(v,t) = \left\{\varrho^E(v,t), \varrho^I(v,t)\right\}$ of a given network, which represents the collection of voltages $\{V_j^Q\}$ within the network by $\varrho^Q(v,t) = \frac{1}{N_Q}\sum_{j=1}^{N_Q}\delta\left(v - V_j^Q(t)\right)$. Let us denote the Liouville distribution by $\rho_{\text{single}}^Q(v,t)$ for the single-neuron voltage distribution. Later, we will draw N_Q independent samples from the single-neuron voltage distribution $\rho_{\text{single}}^Q(v,t)$ to approximate the network voltage configuration $\varrho^Q(v,t)$.

3.2 Multiple-firing events in a conductance-based IF network

There is a wide range of dynamics generated by the conductance-based IF networks (1)–(3), including homogeneity, synchrony and MFEs. The homogeneous dynamics are characterized by largely independent firings and weak temporal correlation between neurons. The highly synchronous dynamics are characterized by repeated large bursts of activity spanning the entire network. These two

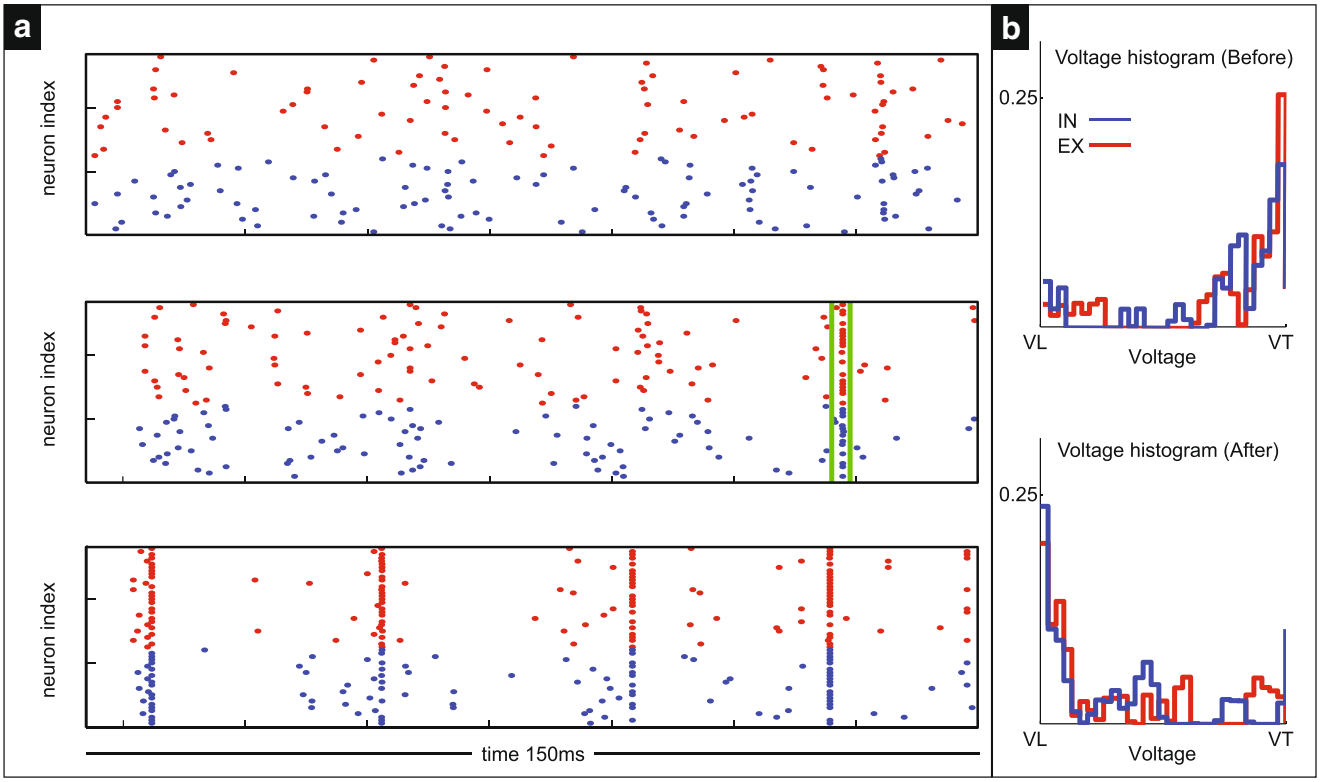

Fig. 1 Multiple-firing events (MFEs). Panel A shows a raster plot of firing activity for the excitatory (red) and inhibitory (blue) neurons in three different networks. Each system has $N_E = 32$, $N_I = 24$, and $S^{II} = 0$, $S^{IE} = 0.003$, $S^{EI} = 0.001$, $S^{EY} = S^{IY} = 0.0055$, $m_{net}^{EY} = m_{net}^{IY} = 2400Hz$. The spikes corresponding to the 56 neurons are shown in red and blue for the excitatory and inhibitory neurons, respectively. For the raster shown on top, we have chosen $S^{EE} = 0.001$. This regime does not frequently generate large magnitude MFEs, and therefore, the dynamics are relatively homogeneous. For the raster shown on the bottom we have increased S^{EE} substantially to 0.0035. Now any excitatory firing event is likely to drive many other neurons to threshold; the network activity is therefore highly synchronous. For the raster shown in the middle we have chosen an intermediate value of $S^{EE} = 0.0026$. The dynamics in this intermediate regime lie in between homogeneity and total synchrony, exhibiting many MFEs of moderate to large sizes. One such MFE is indicated by the two green lines. Panel B plots the excitatory (red) and inhibitory (blue) voltage distributions of the system measured at the green line immediately before (top) and after (bottom) the indicated MFE. Note that, before the MFE, many of the neurons were near V_T. Most of these neurons fire together during the MFE, and are near V_L immediately after the MFE

extreme regimes have been well described and understood by using a few coarse-graining parameters (Ledoux and Brunel 2011; Ostojic and Brunel 2011; Roxin et al. 2011; Litwin-Kumar and Doiron 2012). The intermediate regimes are characterized by brief spurts of spiking activity (see Fig. 1 for an example). These MFEs are an emergent property of the system and is manifested when the system is in a high-gain state. We came upon MFEs in earlier models of the visual cortex, in which we discovered, through a careful benchmarking process, that MFEs are a crucial dynamical mechanism behind many of the phenomena we were able to replicate (Rangan and Young 2013b). In later work, a simpler setting is used to explain how MFEs arise, as well as their potential dynamic consequences (Zhang and Rangan 2015; Rangan and Young 2013a; b; 2014a, b). The importance of MFEs in the biological system motivated us to propose a population-based model to capture the dynamics of MFEs. A crucial observation is that when an MFE occurs, the post-MFE voltage configurations $\varrho^{Q}\left(v, t_{\text{MFE}}^{+}\right)$ tend to be farther away from V_T than the pre-MFE configurations $\varrho^{Q}\left(v, t_{\text{MFE}}^{-}\right)$, particularly after large-sized MFEs. Figure 1 illustrates such an example.

As a consequence of this MFE-induced reorganization, the system is typically much less excitable immediately after an MFE than before. This implies that the firing events that follow in the milliseconds after an MFE tend to be individual firing events (and not MFEs). We will leverage this assumption later in Section 4 and in our final reduction in Section 5, by assuming that the network synaptic activity shortly after each MFE can be well modeled as a Poisson process.

Networks with Only Excitatory Neurons There are some works similar to our MFEs for excitatory-only networks, such as the so-called 'sandpile' model (Bak et al.

1987) (but see also Newhall et al. 2010). Commonly, these models describe a network of pulse-coupled units, each of which increments its own internal state, slowly creeping towards a threshold. Eventually a unit reaches threshold, kicking several other units to threshold, and triggering a chain reaction. A comparison between these MFEs and the sandpile models was made in Hertz and Hopfield (1995). The cascades observed in the sandpile models are similar to the cascades of excitatory firing events that occur during our MFEs. In this case, the magnitudes of MFEs can be computed in a straightforward fashion.

Networks with Excitatory and Inhibitory Neurons The situation is more complicated in networks with both excitatory and inhibitory neurons. First, the excitatory neurons contribute to the initiation of the cascade, and, second, the inhibitory neurons contribute to the termination of the cascade. The competition between excitatory and inhibitory populations on different time scales makes the unfolding of MFEs much more complicated than the 'excitatory-only' cascades in the sandpile model. This added complexity is one reason why we consider all-to-all connectivity as a first step.

The number of excitatory and inhibitory neurons that fire during an MFE are determined by the competition between the E- and I-synaptic couplings, as well as the details of the network's voltage configuration immediately before each MFE. We will use the notation in Zhang et al. (2014a, b) to characterize each MFE via its magnitudes L_E, L_I and depths $\bar{V}^E$, $\bar{V}^I$. Briefly, L_E and L_I are the number of excitatory and inhibitory neurons that spiked during an MFE; and $\bar{V}^E$ and $\bar{V}^I$ are the maximum voltages excitatory and inhibitory neurons could have without participating in the MFE.

We note that the homogeneous, highly synchronous or intermediate regimes studied in this paper seem to resemble the asynchronous irregular (AI), synchronous regular (SR) or synchronous irregular (SI) regimes that are often described following the works of Brunel (2000) and Buzsaki and Wang (2012). However, our IF-networks are in a dynamical regime where the analytical techniques used in Brunel (2000) (Sections 3 and 6.1) are not applicable. In particular, our IF-networks exhibit emergent correlations in the network activity (i.e., MFEs) that cannot be described using a common, time-varying network firing rate. Furthermore, the post-synaptic effect of the global fluctuations has the consequence that our MFEs cannot be well approximated using a time-dependent Poisson process. Hence, many of the phenomena we observe and discuss here do not fall neatly into the categorization scheme of Brunel (2000). For a more detailed discussion, see Zhang and Rangan (2015).

Motivation of Studying Conductance-Based IF Model Generally, conductance-based IF neuronal networks are more realistic versions of Hodgkin-Huxley type of neuronal models (Koch 1999). Here we illustrate the influence of the driving force of the membrane voltage on the following aspects: (i) the voltage distribution, and (ii) the MFE distribution. Figure 2 shows the comparisons of long-time voltage distributions, the second-order statistics (i.e., the MFE magnitude distribution), and the total spectral power (Storch and Zwiers 2001) of the trajectories of mean voltage of excitatory population and inhibitory populations for six network configuration with nearly identical overall firing rate. Although the firing rates are nearly identical, the fine features of the dynamics differ vastly and depend sensitively on the voltage driving force V_E.

As Fig. 2 demonstrates, the fine dynamical features of the conductance-based IF network are much more complex than those of current-based models. This added complexity brings difficulty to the dimensional reduction of population dynamics.

4 The partitioned-ensemble average (PEA)

In this section we first review the standard ensemble average, before introducing the partitioned-ensemble average (PEA) framework for (1)–(3). Specifically, we reduce the system from the joint voltage distribution ρ^Q to two 1D voltage distributions ρ^Q_{single}. For a detailed presentation of the PEA framework, see Zhang et al. (2014a) and Zhang and Rangan (2015).

Ensemble average is one of the standard methods to coarse grain a complicated system (Knight 1972; Abbott and van Vreeswijk 1993; Brunel and Hakim 1999; Omurtag et al. 2000; Nykamp 2000; Cai et al. 2004; Rangan and Cai 2006). However, these standard ensembles are not expected to fully capture the emergent fluctuations arising in IF neuronal networks, which tend to embark on rapid transients only under very specific circumstances. To rationalize the specific assumptions of our PEA-framework, we first observe the following characteristics of MFEs:

1. MFEs are often the main source of dynamic transients in the stationary dynamics;
2. MFEs are initiated whenever one excitatory neuron causes other neurons to fire together;
3. Immediately after an MFE, the system is then often relatively quiescent over the next few ms.

The Partition-Ensemble Average (PEA) Method The above observations motivate our coarse graining: (1) we consider an MFE as a special type of transition in our system, and (ii) the notion of an ensemble average is used to approximate

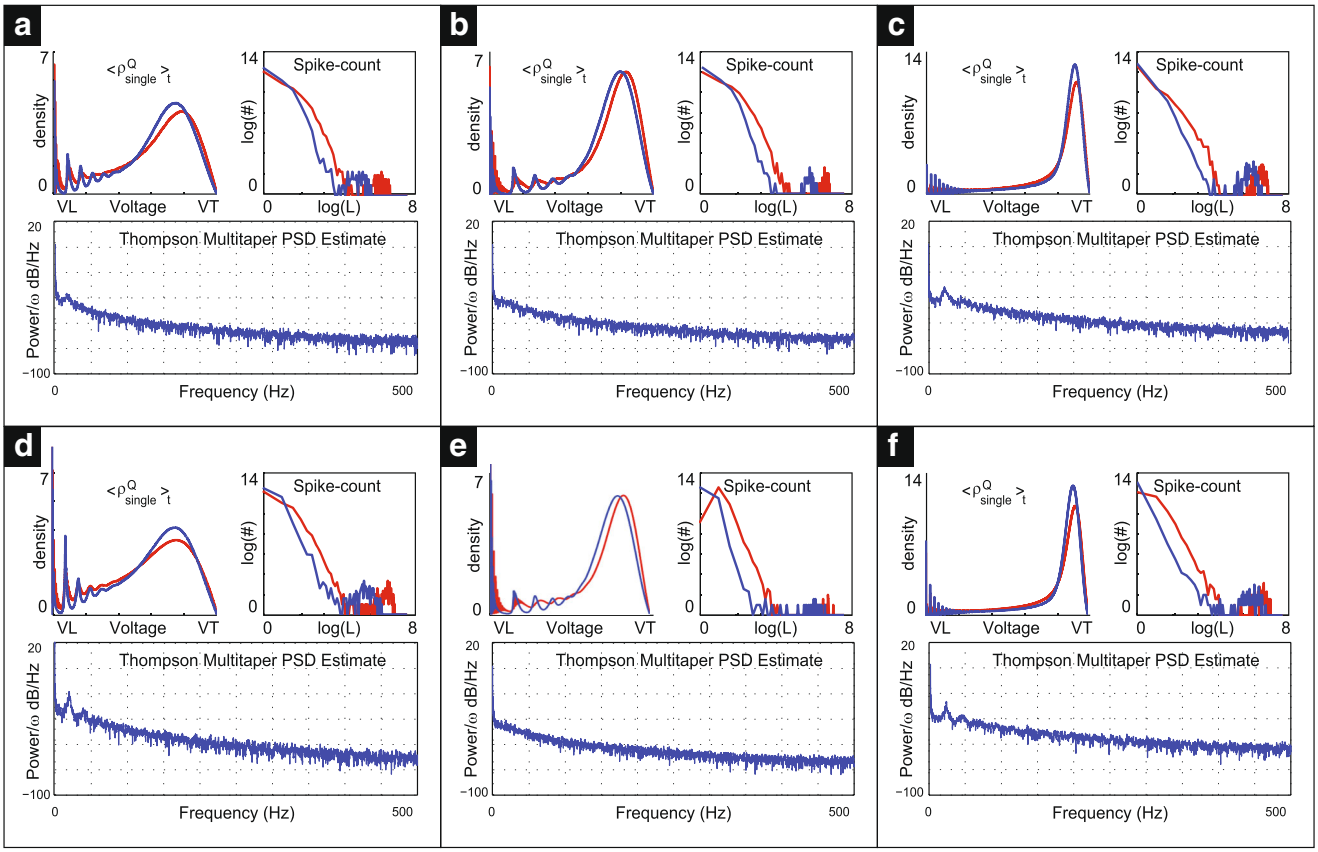

Fig. 2 Comparison between I&F simulations and algorithm-1. Panels A-F show voltage distributions; system firing counts and power spectral densities (Storch and Zwiers 2001) of mean $N_E^{-1}\int v\rho^E_{single}dv + N_I^{-1}\int v\rho^I_{single}dv$. The results in panels A-C are obtained by Algorithm 1 and the results in panels D-F are simulated by the I&F simulation with the same parameters as the Algorithm 1. In each panel, the red color is used to indicate the excitatory neurons and the blue color for inhibitory neurons. In all simulations, we fixed $N_E = N_I = 128$, and $m^{EY}_{net} = 550Hz, m^{IY}_{net} = 540Hz$, $S^{EE} = 0.00144$, $S^{IE} = S^{EI} = 0.0006$, $S^{II} = 0$. In panel A, we take $S^{EY} = 0.018$, $V_E = 14/3$ to obtain the reference system firing rate. In panel B, we change $V_E = 1.5$, $S^{IY} = S^{EY} = 0.102, \alpha S^{EE}, \alpha S^{IE}$ with $\alpha = 5.4$ such that the system firing rate in panel B is identical to the system firing rate in Panel A. In panel C, we also change $V_E = 1.5$ and fix $S^{EY} = S^{IY} = 0.018$, however, we vary the Poisson input rates $m^{EY}_{net} = 4340Hz$, $m^{IY}_{net} = 4180Hz$, and other parameters by $\alpha S^{EE}, \alpha S^{IE}$ with $\alpha = 2.9$ such that the system firing rate in Panel C is identical to the system firing rate in Panel A. Power spectral densities were estimated using Thompson multitaper techniques (see, for instance, Percival and Walden 1993)

a 'typical' system trajectory between two such transitions. To isolate MFEs from single neuron firing events, we define the set of transitions by the magnitude of MFE magnitude $L_E + L_I \geq \bar{L}$. In this paper, we fix $\bar{L} = 2$, which represents the minimum size of the MFE of interest. That is to say, we define an MFE to be an event when one excitatory firing causes at least one other neuron to fire.

Specifically, we track the evolution of the voltage configuration $\boldsymbol{\varrho}$ conditioned on the probability $P(t, t+dt)$ for a MFE to occur. That is to say, we compute the probability that an MFE occurs with a magnitude $L_E + L_I \geq \bar{L}$. Once an MFE occurs at time t, we will take the configuration $\varrho_l(v, t^+)$ of the l-th network immediately afterwards and prepare many identical copies (i.e., ϱ_1, ϱ_2, ...). Then this ensemble Ω would produce an average that, for a short time, captures a typical trajectory. The fidelity of this description will last until one of the networks in Ω (say ϱ_j) generates another MFE, at which time ϱ_j falls into a different sub-ensemble of the Ω-ensemble average. We call this procedure the partitioned-ensemble average (PEA) to differentiate it from the standard ensemble average. (One can refer to Zhang et al. 2014a; Zhang and Rangan 2015 for a more detailed description of the PEA-framework.)

The PEA-dynamics is identical in distribution to the evolution of the original, full ensemble $\Omega(t)$. However, the main difference from the standard ensemble is that the individual trajectories produced by the PEA-dynamics are stochastic. That is to say, both the transition times and the types of MFEs produced during these transitions

are random. The stochastic nature of the PEA-trajectories allows the PEA-dynamics to capture many fine statistical features of the MFEs (e.g., the distribution of MFE magnitudes, the distribution of inter-MFE intervals, and so on).

Assumptions and Approximations Although the PEA-framework offers a conceptually straightforward and dynamically faithful description of the ensemble Ω via the joint voltage distribution, this framework is typically too cumbersome to implement in practice because of the "curse of dimensionality" of an $(N^E + N^I)$-dimensional joint voltage distribution.

To develop a practical scheme, we appeal to the observations of Section 3.2 regarding MFEs, and make the following assumptions: (i) the decorrelation time of neurons in the system is much shorter than the typical inter-MFE intervals, and therefore, (ii) in between MFEs, the individual neurons in the system are not strongly correlated.

These assumptions make it possible to use marginalization to approximate the joint voltage distribution of each ensemble. Upon marginalization, we can evolve the single-neuron voltage distributions $\boldsymbol{\rho}_{single}(v,t) = \left\{\rho^I_{single}(v,t), \rho^E_{single}(v,t)\right\}$ over the k-th time step: $[t, t+dt] = [kdt, kdt+dt]$, then use the information obtained from $\boldsymbol{\rho}_{single}(v, kdt)$ to calculate the transition rate $P_{MFE}(t)$ that represents the probability that an MFE has occurred during that timestep. Using the probability $P_{MFE}(t)$, we draw a Bernoulli random variable π_k to indicate whether or not an MFE has indeed occurred. If $\pi_k = 0$, we infer that no MFE will occur, and thus we keep evolving $\boldsymbol{\rho}_{single}$ forwards in time from kdt to $kdt + dt$ by using a Master-equation $\boldsymbol{f}_{B,single}$, conditioned to ensure that no MFE has occurred. If $\pi_k = 1$, then we infer that an MFE will indeed occur during this timestep and we numerically generate an MFE with L_Q, $\bar{V}^Q$ randomly determined by $\boldsymbol{\rho}_{single}(v, kdt)$. Then we use the voltage distribution immediately after this MFE as the initial condition $\boldsymbol{\rho}_{single}(v, t+dt)$ at timestep $t + dt$, for forward evolution of the population model (which could be a Master equation, a FP equation, or even an augmented ODE system). We evolve the population dynamics until the next occurrence of an MFE.

We summarize the above procedure to a practical algorithm using a Master equation (see also Zhang et al. 2014a; Zhang and Rangan 2015):

In the following, we provide a detailed step-by-step description of our Algorithm-1, namely, how to approximate $P_{MFE}(t)$ and $\bar{\varrho}$, and $\boldsymbol{f}_{B,single}$. For brevity, we leave the detailed derivation of the Master equation for $f_{B,single}$ to Appendix B.

Caculation of $P_{MFE}(t)$ Under the PEA-framework, the probability $P_{MFE}(t)$ is used to compute the Bernoulli random variable π_k over the time interval $[kdt, kdt+dt]$, and can be expressed by

$$P_{MFE}(t) = dt \cdot N_E \cdot m^E_{single}(kdt) \cdot [1 - q(kdt)], \tag{7}$$

where $m^Q_{single}(t)$ denotes the single-neuron firing rates, and $q(kdt)$ represents the probability that, given a single excitatory neuron at threshold, the other $N_E - 1$ excitatory neurons and N_I inhibitory neurons drawn from the $\rho^Q(v, kdt)$ are far enough away from threshold to preclude an MFE:

$$q(kdt) = \left[\int_{-\infty}^{T(V_T, S^{EE})} \rho^E(v, kdt)\, dv\right]^{N_E - 1} \times \left[\int_{-\infty}^{T(V_T, S^{IE})} \rho^I(v, kdt)\, dv\right]^{N_I}.$$

Conversely, $(1 - q(kdt))$ represents the probability that the spiking of a single excitatory neuron can cause *at least* one other neuron to reach threshold.

Algorithm 1

Input the 10-dimensional parameters: Network size, N_I and N_E; Feedforward input rates, m^{IY}_{net}, m^{EY}_{net} and input strengths, S^{IY}, S^{EY}; Network synaptic coupling strengths, S^{II}, S^{IE}, S^{EI}, S^{EE}.

1. Initialize $\boldsymbol{\rho}_{single}(v, 0)$ and set $k = 0$;
2. At each time-step $[kdt, kdt+dt]$, draw a Bernoulli random variable π_k with success probability $P_{MFE}(t)$ determined by $\boldsymbol{\rho}_{single}(v, kdt)$ - see Eq. (7) below;
3. If the Bernoulli random variable $\pi_k = 0$, evolve $\boldsymbol{\rho}_{single}$ using the Master equation $\boldsymbol{f}_{B,single}$ - see Eq. (37). Set $k := k + 1$ and go back to step 2;
4. When $\pi_k = 1$, pause evolving the Master equation;
5. Use $\boldsymbol{\rho}_{single}(v, kdt)$ to sample an MFE. Then, given the sampled MFE, draw a single post-MFE configuration $\bar{\varrho}_{single}$;
6. Set $\boldsymbol{\rho}_{single}(v, kdt + dt)$ equal to $\bar{\varrho}_{single}$. Namely, take $\bar{\varrho}_{single}$ as the initial value for forward evolution. And finally, back to step 2.

Sample an MFE and Approximating $\bar{\varrho}$ If we find that $\pi_k = 1$ at time $t = kdt$ in step 2, then we proceed to step 5, and draw an MFE of magnitude $\geq \bar{L}$ from the distribution of possible MFEs. Under the PEA-framework, we can simply produce a single MFE drawn from this measure. To construct the measure on all possible MFEs, we can repeatedly sample the voltage configurations $\boldsymbol{\varrho}$ from

$\boldsymbol{\rho}_{single}(v,t)$, then use the spike resolution discussed in Appendix A to determine the size L_Q of the MFE associated with each configuration given a single excitatory neuron at threshold.

Derivation of the Master Equation $f_{B,single}$ in Appendix B we derive the Master equation $\boldsymbol{f}_{B,single}$ that governs the dynamics responsible for the nucleation and generation of MFEs. This Master equation $\boldsymbol{f}_{B,single}$ reduces to a standard Master Eq. (8) (see below) when the dynamics is homogeneous. In this paper, we derive a reduction of spiking neuronal dynamics from the standard Master Eq. (8) instead of $\boldsymbol{f}_{B,single}$. This derivation is a much more simplified and straightforward version of the one in Zhang and Rangan (2015).

5 A reduction of the spiking neuronal network

In this section, we present a dimensional reduction of the conductance-based IF network from the standard Master equation to an augmented low-dimensional ODE system. The augmented ODE system inherits the parameters of the original IF neuronal networks without the introduction of any new parameter.

The Standard Master Equation Similar to the ensemble average methods developed in Knight (1972), Abbott and van Vreeswijk (1993), Brunel and Hakim (1999), Omurtag et al. (2000), Nykamp (2000), Cai et al. (2004), and Rangan and Cai (2006), when the dynamics of spiking network is homogeneous and pairwise neuronal correlations are negligible, we can reduce the IF network (1)–(3) to a standard Master equation of the form

$$\begin{aligned}\partial_t \rho^Q(v,t) = {} & g_L \partial_v \left[(v-V_L)\rho^Q(v,t)\right] \\ & + m_{net}^{QY}(t)\cdot\left[\rho^Q\left(T(v,S^{QY}),t\right)\cdot T'(v,S^{QY}) - \rho^Q(v,t)\right] \\ & + N_E m^E(t)\cdot\left[\rho^Q\left(T(v,S^{QE}),t\right)\cdot T'(v,S^{QE}) - \rho^Q(v,t)\right] \\ & + N_I m^I(t)\cdot\left[\rho^Q\left(T(v,S^{QI}),t\right)\cdot T'(v,S^{QI}) - \rho^Q(v,t)\right] \\ & + \mathcal{S}^Q(t)\cdot\delta(V-V_R), \end{aligned} \tag{8}$$

where $\rho^Q(v,t)$ represents the single-neuron voltage distribution at time t, $T(v,\cdot)$ is defined in Eq. (6), and the source $\mathcal{S}^Q(t)$ is the fraction of the flux across threshold which is then reset to V_R. The derivation of Eq. (8) is detailed in Appendix C.

Fokker-Planck Equation For further theoretical analysis, we now discuss how to approximate the Master Eq. (8) by a FP equation. In the mean-field limit, when pairwise neuronal correlations can be neglected, the evolution of the voltage probability distribution function can be transformed into a FP-type equation (Brunel and Hakim 1999; Fourcaud and Brunel 2002) (for more recent work using probability theory and field-theoretical methods see Robert and Touboul (2016), Touboul (2014), Buice and Chow (2007), and Bressloff (2015) and references therein).

Let $s = e^{S^{QY}} - 1$, $s_1 = e^{S^{QE}} - 1$, $s_2 = e^{S^{QI}} - 1$, we can approximate the Master Eq. (8) to a FP-type equation (see the detailed derivation in Appendix D)

$$\partial_t \rho^Q(v,t) + g_T^Q \partial_v J(v;\rho^Q) = 0, \tag{9}$$

where

$$J(v;\rho^Q) = -(v-\mu^Q)\rho^Q - \frac{\sigma^Q(v)}{2}\partial_v\rho^Q - \zeta^Q\int_{-\infty}^{v}\rho^Q(s,t)ds, \tag{10}$$

$$g_T^Q = g_L + m_{net}^{QY}(t)s(1-s^2) + m^E(t)N_E s_1(1-s_1^2) + m^I(t)N_I s_2(1-s_2^2), \tag{11}$$

$$\mu^Q = \frac{1}{g_T^Q}\left[g_L V_L + m_{net}^{QY}(t)s(1-s^2)V_E + m^E(t)N_E s_1(1-s_1^2)V_E + m^I(t)N_I s_2(1-s_2^2)V_I\right], \tag{12}$$

$$\begin{aligned}\sigma^Q(v) = {} & \frac{1}{g_T^Q}\Big[m_{net}^{QY}(t)(1+s)s^2(v-V_E)^2 + N_E m^E(t)(1+s_1)s_1^2(v-V_E)^2 \\ & + N_I m^I(t)(1+s_2)s_2^2(v-V_I)^2\Big], \end{aligned} \tag{13}$$

$$\zeta^Q = \frac{1}{g_T^Q}\left[m_{net}^{QY}(t)s^3 + N_E m^E(t)s_1^3 + N_I m^I(t)s_2^3\right]. \tag{14}$$

The single-neuron firing rate m^Q is obtained by the flux at threshold, namely,

$$m^Q(t) = g_T^Q J(V_T,\rho^Q,t). \tag{15}$$

The boundary conditions for Eq. (9) satisfy

$$\rho^Q(V_T,t) = \rho^Q(V_I,t) = 0. \tag{16}$$

Since the potential of each neuron will be reset, immediately after firing, the flux jumps by

$$g_T^{\mathcal{Q}} J(V_R^+; \rho^{\mathcal{Q}}, t) - g_T^{\mathcal{Q}} J(V_R^-; \rho^{\mathcal{Q}}, t) = m^{\mathcal{Q}}(t). \tag{17}$$

Equilibrium Solution We now consider the equilibrium solution $\rho_{Eq}^{\mathcal{Q}}$ to Eq. (9), namely, the solution to

$$\partial_v \left\{ (v - \mu^{\mathcal{Q}}) \rho_{Eq}^{\mathcal{Q}} + \frac{\sigma^{\mathcal{Q}}(v)}{2} \partial_v \rho_{Eq}^{\mathcal{Q}} \right\} + \gamma \rho_{Eq}^{\mathcal{Q}} = 0. \tag{18}$$

By integrating (18) over the interval $[v, V_T]$ and using the boundary conditions (16), we have

$$(v - \mu^{\mathcal{Q}}) \rho_{Eq}^{\mathcal{Q}} + \frac{\sigma^{\mathcal{Q}}(v)}{2} \partial_v \rho_{Eq}^{\mathcal{Q}} = -m^{\mathcal{Q}} / g_T^{\mathcal{Q}} e^{\gamma(V_T - v)}, \tag{19}$$

which can be rewritten as

$$\frac{2(v - \mu^{\mathcal{Q}})}{\sigma^{\mathcal{Q}}(v)} \rho_{Eq}^{\mathcal{Q}} + \partial_v \rho_{Eq}^{\mathcal{Q}} = -\frac{2m^{\mathcal{Q}}}{g_T^{\mathcal{Q}} \sigma^{\mathcal{Q}}(v)} e^{\gamma(V_T - v)}. \tag{20}$$

To simplify further, we rewrite the diffusion term $\sigma^{\mathcal{Q}}(v)$ as

$$\sigma^{\mathcal{Q}}(v) = av^2 + bv + c, \tag{21}$$

where the coefficients are given by

$$a = \left[m_{net}^{\mathcal{QY}} s^2 (1 + s)) + m^E N_E s_1^2 (1 + s_1) + m^I N_I s_2^2 (1 + s_2) \right] / g_T^{\mathcal{Q}}, \tag{22}$$

$$b = -\frac{2}{g_T^{\mathcal{Q}}} \left[m_{net}^{\mathcal{QY}} s^2 (1 + s)) V_E + m^E N_E s_1^2 (1 + s_1) V_E + m^I N_I s_2^2 (1 + s_2) V_I \right], \tag{23}$$

$$c = \left[m_{net}^{\mathcal{QY}} s^2 (1 + s)) V_E^2 + m^E N_E s_1^2 (1 + s_1) V_E^2 + m^I N_I s_2^2 (1 + s_2) V_I^2 \right] / g_T^{\mathcal{Q}}. \tag{24}$$

Defining $\theta(v)$ by the integral

$$\theta(v) \equiv \int \frac{2(v - \mu^{\mathcal{Q}})}{\sigma^{\mathcal{Q}}(v)} dv = \begin{cases} \frac{1}{a} \ln \sigma^{\mathcal{Q}}(v) - \frac{2b + 4a\mu^{\mathcal{Q}}}{a\sqrt{4ac - b^2}} \arctan \frac{2av + b}{\sqrt{4ac - b^2}}, & \text{if} \quad 4ac - b^2 > 0, \\ \frac{1}{a} \ln \sigma^{\mathcal{Q}}(v) + \frac{2b + 4a\mu^{\mathcal{Q}}}{a(2av + b)}, & \text{if} \quad 4ac - b^2 = 0. \end{cases}$$

Then Eq. (20) becomes

$$\partial_v \left[e^{\theta(v)} \rho_{Eq}^{\mathcal{Q}} \right] = -\frac{2m^{\mathcal{Q}}}{g_T^{\mathcal{Q}} \sigma^{\mathcal{Q}}(v)} e^{\zeta^{\mathcal{Q}}(V_T - v) + \theta(v)}. \tag{25}$$

Integrating (25) over the interval $[v, V_T]$, we obtain the equilibrium distribution of Eq. (9):

$$\rho_{Eq}^{\mathcal{Q}}(v) = \begin{cases} \frac{2m^{\mathcal{Q}}}{g_T^{\mathcal{Q}}} e^{-\theta(v)} \int_v^{V_T} \frac{1}{\sigma^{\mathcal{Q}}(x)} e^{\zeta^{\mathcal{Q}}(V_T - x) + \theta(x)} dx, & v \in [V_R, V_T], \\ \frac{2m^{\mathcal{Q}}}{g_T^{\mathcal{Q}}} e^{-\theta(v)} \int_{V_R}^{V_T} \frac{1}{\sigma^{\mathcal{Q}}(x)} e^{\zeta^{\mathcal{Q}}(V_T - x) + \theta(x)} dx, & v \in [-\infty, V_R), \end{cases} \tag{26}$$

where the single-neuron firing rate $m^{\mathcal{Q}}$ at the equilibrium can be obtained by normalizing $\rho_{Eq}^{\mathcal{Q}}(v)$.

In the following we use the FP equation to derive an augmented system of ODEs.

Moment Equation Here we focus on reducing the FP Eq. (9) by introducing voltage moments $\mathcal{M}_k^{\mathcal{Q}}$. Our goal is to faithfully capture the features of the heterogeneous dynamics of neuronal networks by evolving a low-dimensional system from the initial time t_0 onwards given only the initial conditions $\mathcal{M}^{\mathcal{Q}}(t_0)$ and firing rates $m^{\mathcal{Q}}(t_0)$. Let us define the k^{th} moment by

$$\mathcal{M}_k^{\mathcal{Q}} = \int_{-\infty}^{V_T} v^k \rho^{\mathcal{Q}}(v) dv,$$

where the single-neuron voltage distribution $\rho^{\mathcal{Q}}(v)$ satisfies the FP Eq. (9)

$$\partial_t \rho^{\mathcal{Q}} = g_T^{\mathcal{Q}} \partial_v \left\{ (v - \mu^{\mathcal{Q}}) \rho^{\mathcal{Q}} + \frac{\sigma^{\mathcal{Q}}(v)}{2} \partial_v \rho^{\mathcal{Q}} \right\} + g_T^{\mathcal{Q}} \zeta^{\mathcal{Q}} \rho^{\mathcal{Q}}. \tag{27}$$

Multiplying Eq. (27) with v^k, and integrating by parts over the interval $[-\infty, V_T]$, we obtain that the k-th moment evolves according to

$$\begin{aligned} \frac{d\mathcal{M}_k^{\mathcal{Q}}(t)}{dt} = &-(V_T)^k m^{\mathcal{Q}}(t) - g_T^{\mathcal{Q}} k \left(1 - \frac{(k+1)a}{2} - \frac{\zeta^{\mathcal{Q}}}{k} \right) \mathcal{M}_k^{\mathcal{Q}} \\ &+ g_T^{\mathcal{Q}} k \left(\mu^{\mathcal{Q}} + \frac{kb}{2} \right) \mathcal{M}_{k-1}^{\mathcal{Q}} + g_T^{\mathcal{Q}} \frac{k(k-1)c}{2} \mathcal{M}_{k-2}^{\mathcal{Q}}. \end{aligned} \tag{28}$$

Here the 0-th moment $\mathcal{M}_0^{\mathcal{Q}} = 1$ and we set $\mathcal{M}_{-1}^{\mathcal{Q}} = 0$. The evolution of Eq. (28) depends on the coefficients $g_T^{\mathcal{Q}}$ given in Eq. (11), $\mu^{\mathcal{Q}}$ given in Eq. (12), $\sigma^{\mathcal{Q}}$ given in Eq. (13), and $\zeta^{\mathcal{Q}}$ given in Eq. (14), as well as the single-neuron firing rate $m^{\mathcal{Q}}$ given in Eq. (15). Importantly, we point out that (28) does not depend on the moments higher than k, but it is *not* a closed system since $m^{\mathcal{Q}}$ is determined by the voltage density $\rho^{\mathcal{Q}}$ at the threshold V_T.

Maximum Entropy Method The system of ODEs (28) is not closed because we cannot compute directly the network

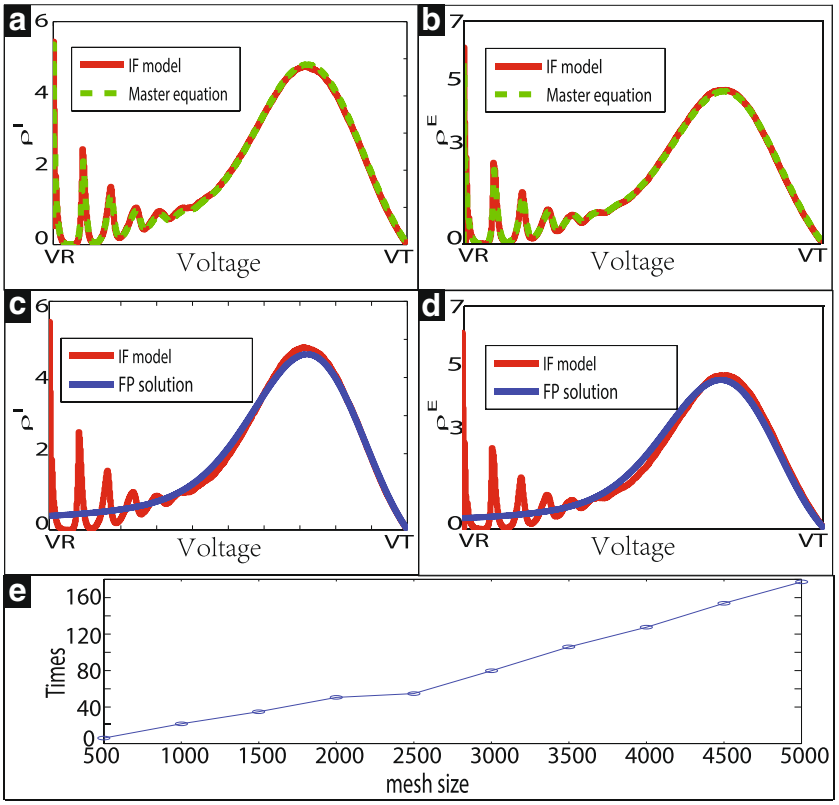

Fig. 3 A nearly homogeneous scenario for our PEA-framework. For this network we have set $N_E = N_I = 128$ with $S^{EE} = S^{EI} = S^{IE} = 0.0006$, $S^{II} = 0$, $m_{net}^{EY} = 550Hz$, $m_{net}^{IY} = 540Hz$, and $S^{EY} = S^{IY} = 0.018$. In panels **a** and **b** we compare the steady-state voltage distributions for $\rho^E(v)$ and $\rho^I(v)$, respectively. The red line is achieved by IF model and the green dash line by the Master equation. In panels **c** and **d** we compare the steady-state voltage distributions for $\rho^E(v)$ and $\rho^I(v)$, respectively. The red line is achieved by IF equation and the blue line by Fokker-Planck equation. In panel E, we compare ratios by the computational time by Fokker-Planck equation/the computational time by Master equation with different number of mesh points

firing rate. Obviously, we need to compute the instantaneous voltage distribution $\rho^{\mathcal{Q}}(v,t)$, which can be then used to update the firing rate $m^{\mathcal{Q}}(t)$, allowing the closure of the moment hierarchy.

However, at each time, there are many voltage distributions $\rho^{\mathcal{Q}}(v,t)$ that are compatible with the given moments $\mathcal{M}_k^{\mathcal{Q}}(t)$. Thus, from amongst these possible voltage distributions, we need to select one that is most 'compatible' with the network dynamics. Here, we choose to use the one 'closest' to the system's equilibrium solution.

Thus, we introduce the maximum entropy method to compute the 'most likely' voltage-distribution $\rho_{me}^{\mathcal{Q}}(v,t)$ by

$$\begin{aligned}\rho_{me}^{\mathcal{Q}}(v,t) &\equiv \arg\max_{\rho} H(\rho)\\ &= \arg\max_{\rho}\left\{-\int_{-\infty}^{V_T}\rho(v,t)\log\left(\rho^{\mathcal{Q}}(v,t)/\rho_{Eq}^{\mathcal{Q}}(v)\right)dv\right\},\\ &\quad \text{subject to}\quad \int_{-\infty}^{V_T} v^k\rho^{\mathcal{Q}}(v,t)dv-\mathcal{M}_k(t)=0,\\ k &= 0,1,\cdots,N,\end{aligned}\tag{29}$$

where the equilibrium solution $\rho_{Eq}^{\mathcal{Q}}$ is given by Eq. (26). To solve the optimization problem (29), we construct the Lagrangian function

$$\mathcal{L}(\rho,\lambda^{\mathcal{Q}}) = H(\rho) + \sum_{j=0}^{N}\lambda_j^{\mathcal{Q}}\cdot\left(\int_{-\infty}^{V_T} v^k\rho^{\mathcal{Q}}(v,t)dv-\mathcal{M}_k(t)\right),\tag{30}$$

where $\lambda^{\mathcal{Q}} = \left[\lambda_0^{\mathcal{Q}},\lambda_1^{\mathcal{Q}},\cdots,\lambda_N^{\mathcal{Q}}\right]$ are the Lagrange multipliers. A necessary and sufficient condition for $\rho_{me}^{\mathcal{Q}}$ to be a maximizer of problem (29) is that there must exist a set of parameters $\lambda^{\mathcal{Q}}$ such that $\mathcal{L}'(\rho,\lambda^{\mathcal{Q}})(\delta\rho) = 0$ for all $\delta\rho$. Thus we can obtain the classical solution of Eq. (29),

$$\rho_{\text{me}}^{\mathcal{Q}}(v,t) = \rho_{Eq}^{\mathcal{Q}}\cdot\exp\left(\sum_{j=0}^{N}\lambda_j^{\mathcal{Q}}v^j-1\right).\tag{31}$$

Substituting (31) into the constraints

$$\int_{-\infty}^{V_T} v^k\rho_{\text{me}}^{\mathcal{Q}}(v,t)dv-\mathcal{M}_k(t)=0,\quad k=0,2,\cdots,N,\tag{32}$$

we obtain the values of $\lambda^{\mathcal{Q}}$. Noting the relationship $m^{\mathcal{Q}}(t) = g_T^{\mathcal{Q}}J(V_T,\rho^{\mathcal{Q}},t)$ in Eq. (15) and replacing $\rho^{\mathcal{Q}}$ by $\rho_{\text{me}}^{\mathcal{Q}}(v,t)$, we immediately have the single-neuron firing rate

$$m^{\mathcal{Q}}(t) = \frac{g_T^{\mathcal{Q}}}{C}\exp\left(\sum_{j=0}^{N}\lambda_j^{\mathcal{Q}}(V_T)^j\right),\tag{33}$$

where C is the normalization factor of equilibrium solution (26) and is given by

$$C = \int_{-\infty}^{V_T} e^{-\theta(v)}\int_{\max\{v,V_R\}}^{V_T}\frac{1}{\sigma^{\mathcal{Q}}(x)}e^{\zeta^{\mathcal{Q}}(V_T-x)+\theta(x)}dxdv.$$

An example of the equilibrium solution is shown in Fig. 3c, d. We remark that the equilibrium solution is not quite a

Gaussian, because the mechanisms of firing and resetting prevent the voltage values from rising above V_T, and furthermore, leading to an influx of probability at V_L.

Algorithm 2

Input the 10-dimensional parameters: Network size, N_I and N_E; External input rates, m_{net}^{IY}, m_{net}^{EY} and coupling strengths S^{IY}, S^{EY}; Synaptic coupling strengths, S^{II}, S^{IE}, S^{EI}, S^{EE}.

1. At each time-step $[t, t+dt]$, we consider $m^{\mathcal{Q}}(t)$, $\mathcal{M}_k^{\mathcal{Q}}(t)(k=1,\cdots,N)$ as given;
2. Given $m^{\mathcal{Q}}(t)$, we use Eq. (38) to calculate $m_{net}^{\mathcal{Q}R}\left(t; m^{\mathcal{Q}}\right)$, as well as use Eqs. (11)–(14) to calculate $g_T^{\mathcal{Q}}(t)$, $\mu^{\mathcal{Q}}(t)$, $\sigma^{\mathcal{Q}}(t)$, $\zeta^{\mathcal{Q}}(t)$, then compute $\mathcal{M}_k^{\mathcal{Q}}(t+dt)$ by Eq. (28) with a first-order Euler method; and finally calculate the equilibrium distribution $\rho_{Eq}^{\mathcal{Q}}(t)$ by Eq. (26);
3. Given $\mathcal{M}_k^{\mathcal{Q}}(t+dt)$ and $\rho_{Eq}^{\mathcal{Q}}(t)$, we obtain the Lagrange multipliers $\lambda^{\mathcal{Q}}$ by solving Eq. (32), then compute the maximum entropy distribution $\rho_{me}^{\mathcal{Q}}(v, t+dt)$ using (31), and single neuron firing rate $m^{\mathcal{Q}}(t+dt)$ using (33);
4. To calculate the probability $P_{\mathrm{MFE}}(t+dt)$ generating an MFE, we use $\rho_{me}^{\mathcal{Q}}(t+dt)$ from step 3 to replace $\rho_{single}^{\mathcal{Q}}$, and $m^{\mathcal{Q}}(t+dt)$ to replace $m_{\mathrm{single}}^{\mathcal{Q}}(t+dt)$ in Eq. (7);
5. Taking $P_{\mathrm{MFE}}(t+dt)$ as the success probability, we draw a Bernoulli random variable π to determine if either
   (a) $\pi = 0$, in which case no MFE occurs during this time-step, we do nothing, go back to step 1;
   (b) $\pi = 1$, in which case an MFE occurs. We sample an MFE from $\rho_{me}^{\mathcal{Q}}(t+dt)$ and update $m^{\mathcal{Q}}$ and $\mathcal{M}_k^{\mathcal{Q}}$ at time $t+dt$ appropriately; see the details in Section 4, and go back to step 1.

Calculation of the Equilibrium An important issue regarding the maximum-entropy method is the construction of the equilibrium distribution when the drift and diffusion coefficients $\mu^{\mathcal{Q}}, \sigma^{\mathcal{Q}}$ are not fixed in time. If $m^{\mathcal{Q}}(t)$ is small and $\mu^{\mathcal{Q}}(t), \sigma^{\mathcal{Q}}(t)$ are changing slowly, we can approximate $\rho_{Eq}^{\mathcal{Q}}(v,t)$ locally in time with these information. Thus H can be considered as an approximate entropy function to capture the local behavior of $\rho^{\mathcal{Q}}(v,t)$ over time. In fact, $\rho^{\mathcal{Q}}(v,t)$ converges to $\rho_{Eq}^{\mathcal{Q}}(v,t)$ on a relatively longer timescale, and both $\rho^{\mathcal{Q}}(v,t)$ and $\rho_{Eq}^{\mathcal{Q}}(v,t)$ will eventually settle to the long-time global equilibrium distribution $\tilde{\rho}_{Eq}(v)$ on a slower timescale. On the other hand, we make use of the maximum-entropy method to achieve closure of the moment hierarchy Eqs. (28) within the context of the PEA-framework. Since the occasional MFEs lead to large transient changes in the density $\rho^{\mathcal{Q}}(v,t)$, the $\tilde{\rho}_{Eq}^{\mathcal{Q}}(v)$ will never actually be achieved, and hence, it makes sense to use the local equilibrium distribution $\rho_{Eq}^{\mathcal{Q}}(v,t)$ to define H within our maximum-entropy method.

5.1 Summary of moment-reduction: Algorithm2

In this section we summarize the moment reduction within the PEA-framework. In the examples to follow, we demonstrate that by using a 4-variable moment closure (membrane potential averages and variances of the excitatory and inhibitory populations, $\{\mathcal{M}_1^E, \mathcal{M}_2^E, \mathcal{M}_1^I,$ and $\mathcal{M}_2^I\}$), we can capture many essential features of MFEs. The following practical implementation is denoted as Algorithm-2.

6 Numerical examples

In this section, the trajectories of various IF networks are compared with the associated trajectories of our coarse-graining methods. We will use the terms 'P1' to refer to Algorithm 1 and 'P2' to Algorithm 2.

6.1 Ideal scenarios: homogeneity and synchrony

We expect Algorithm-1 to be an excellent description of the IF network when our major assumptions are well founded, i.e, two special cases: homogeneity and total synchrony.

The first case where our assumptions are valid is when the dynamic regime is homogeneous. When the coupling strengths $S^{\mathcal{Q}\mathcal{Q}'}$ are very small relative to the typical distance between any neuron's voltage and threshold, the dynamics is homogeneous and the neurons are nearly uncorrelated. The probability of one excitatory firing event causing another firing event is nearly zero and there are no MFEs. In this limit, the PEA-framework reduces to the standard ensemble average dynamics (Sirovich et al. 2000; Cai et al. 2006). Thus, in the limit of weak coupling, our PEA-framework captures the statistics of the network by construction (see, for instance, panels a and b in Fig. 3). The panels c and d in Fig. 3 show the comparison of equilibrium solutions between IF model and FP equation. Panel e in Fig. 3 shows the ratios of the computational times between FP equation and Master equation. We note that one needs to perform thousands to ten of thousands samples by simulating the neuronal network using Monte Carlo methods to obtain the average distribution and average firing rate, thus here we do not directly compare the CPU time. One can see that both of the reduced models can efficiently capture the corresponding voltage distribution and firing rate of the neuronal networks, but the Master equation is more accurate than the FP equation, and is faster when the number of mesh points is larger. Hence we use the Master equation

in numerical simulations of Algorithm-1. However, as we have shown, the FP equation plays an important role for the further reduction to Algorithm-2.

The other limiting case where our assumptions are valid is when MFEs are very rare relative to both the leakage timescale (20ms in our numerical examples) and the typical inter-event-interval of the external Poisson input (say, when the inter-spike interval is tens to a few hundred milliseconds). Because the neurons in the network almost do not interact between firing events, the configuration of the network immediately prior to each firing event will be well represented by a direct-product of single-neuron distributions. If, in addition, S^{EE} is sufficiently large, then any single firing event will cause an MFE. Hence, in this scenario, by construction, our PEA-framework will perform well to capture the statistics of the MFEs. An example of a regime close to this idealized scenario is given in Fig. 4. The panels *A* and *B* shows 10s traces of the firing events of an IF network and the Master equation, respectively. In the inset of the panels *A* and *B* we zoom in the system activities to show that an excitatory neuron either fires independently or causes all other neurons to fire synchronously. In panel *C* we collect a histogram of inter-MFE-intervals (i.e., inter-spike intervals for any given neuron in the network). In the inset of panel *C* we show the mean and standard-deviation of this histogram. In panel *D*, the long-term voltage distribution is compared by averaging the voltage distribution for 10s interval.

It is important to note that the standard ensemble average will settle to a steady state for this regime, but the long-time evolution of the standard ensemble average will not reflect the continuous, strong stochastic fluctuations exhibited in this highly synchronous regime of If networks.

6.2 More realistic scenarios: between homogeneity and synchrony

As we have seen above, within the PEA-framework, our algorithm-1 is capable of capturing both homogeneous regimes and regimes with rare synchronous firing-events. Now we investigate the dynamic regimes between these two limiting scenarios, where our major assumptions become less obviously satisfied with the stochastic occurrence of MFEs. Nevertheless, as we will illustrate below, both algorithm-1 and algorithm-2 can qualitatively capture the statistical features of the dynamic fluctuations in these regimes.

Figure 5 shows a typical regime with many large MFEs that is not quite as synchronous as that in Fig. 4. Both P1 and P2 trajectories can reasonably capture the stationary statistics of the MFEs within such a regime. Other measures of dynamical fluctuations, such as the power spectral density (PSD) of the average network voltage and the variance in the time-averaged voltage distributions are also qualitatively represented within the PEA-framework.

Figure 6 shows typical regimes with lower frequency, medium-to-large sized MFEs. Again, the PEA-framework performs well in capturing the statistics of the fluctuations.

For these intermediate regimes, it is impossible to match exactly the statistics of individual IF-trajectory because the dynamics are very sensitive to the system parameters (e.g., S^{QR}, m_{net}^{QR}, etc.; see, for instance, the detailed discussion in Bornholdt and Rohl 2003; Werner 2007; Poil et al. 2012). As these parameters are varied, the corresponding emergent dynamical transients can change dramatically. Figures 5–6 only give a glimpse into the wide variety of dynamic regimes a conductance-based spiking network can support.

Our study of this dynamical landscape is far from exhaustive, but we can carry out a somewhat structured investigation by fixing many of the system parameters and varying only a few. For illustration we choose a network with $N_E = N_I = 128$, $m_{net}^{EY} = 550Hz$, $m_{net}^{IY} = 540Hz$, and $S^{EY} = S^{IY} = 0.018$, and vary a few of the coupling strengths. We fix $S^{II} = 0$, and vary S^{EE} simultaneously from 0.00125 to 0.00144. We fix S^{EI} and S^{IE} to be equal to and vary them simultaneously from 0.0006 to 0.0015. Increasing S^{EE} will increase the prevalence of MFEs, whereas increasing either S^{EI} or S^{IE} will do the opposite (Rangan and Young 2013a). By scanning this two-dimensional projection of parameter space, we can reproduce synchronous dynamics when the excitation dominates the inhibition, and we can produce homogeneous dynamics when the inhibition dominates the excitation. In between these two extremes lie the intermediate regimes which produce many MFEs of varying magnitudes. The stationary states of these intermediate regimes are far from quiescent, and exhibit a wide range of fluctuations, many of which correspond to γ-band oscillations (with characteristic frequencies of 30-80Hz).

Figure 7 shows the above 2-dimensional slice through parameter space. For each point we simulate the IF network and calculate the corresponding P1- and P2-trajectories. For each simulation we measure the power in the γ-band of the average system voltage, which is computed after we simulate the system for a sufficiently long time so that any transients due to initial conditions are negligible. The γ-band power as a function of system parameters is plotted for the IF, P1- and P2-algorithms. The PEA-framework can well capture the overall strength of the γ-fluctuations produced by this network with these particular parameters; however, it is important to note that the long-time evolution of the standard ensemble average does not reflect the effects of these stationary statistics.

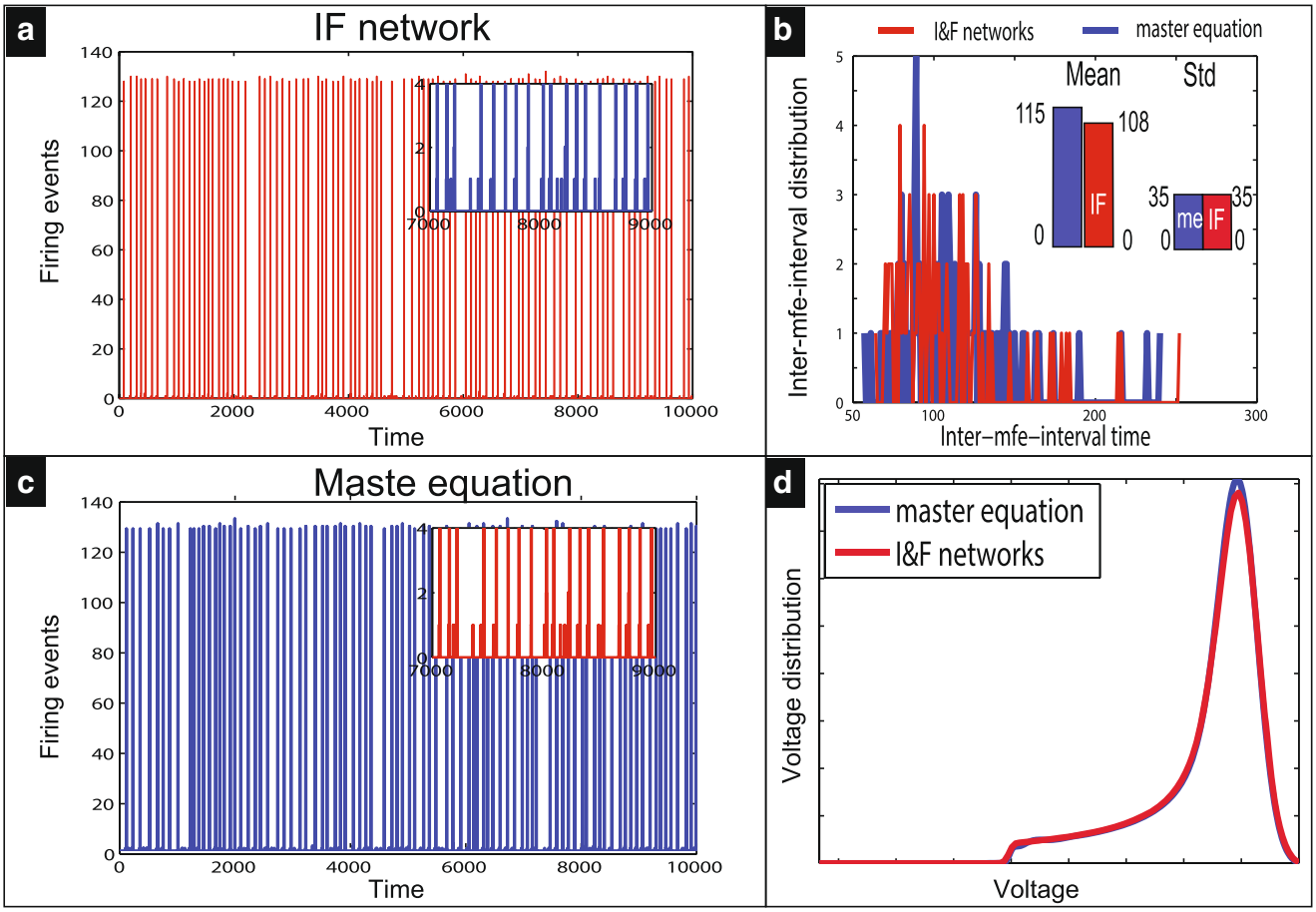

Fig. 4 A nearly ideal scenario for our PEA-framework. For this excitatory-only network we have set $N_E = 128$, with $S^{EE} = 0.006$, $m_{net}^{EY} = 4000Hz$, and $S^{EY} = 0.0026$. In panels **a** and **b** we give examples of the system's activity, and show 10s traces of the IF (panel **a**), Master equation (panel **b**) trajectories. In panel **c** we collect a histogram of inter-MFE-intervals. In the inset, we show the mean and standard-deviation for this histogram. In panel **d**, the voltage distribution are compared by averaging the voltage distribution for 10s computational interval. Note that our algorithms perform well to capture the relevant statistics of this dynamical regime

7 Discussion

The vast range of neuronal network dynamics presents an enormous challenge to computational neuroscientists. Ever more detailed neurophysiological datasets and neuronal network simulations reveal interactions on multiple spatial and temporal scales that also participate in essential brain functions. The observed network dynamics can be quite complex and exhibits stochastic fluctuations incorporating strong, transient correlations. Unfortunately, many population methods cannot capture even the lowest order statistics associated with these dynamical regimes, and consequently, the underlying fluctuating activity cannot effectively be described by standard ensemble averages.

A challenging issue for theoretical neuroscience is to develop a single mathematical framework that can effectively reduce and capture a broad range of network dynamics, ranging from homogeneity to synchrony. Here we focus on MFEs because of the belief that they are the main drive underlying the emergent transient fluctuations within the stationary states of complex neuronal networks (see, for instance, Mazzoni et al. 2007; Shew et al. 2011; Dehghani et al. 2012; Rangan and Young 2013b; Poil et al. 2012; DeVille and Zheng 2014). Previously, we examined in detail the MFEs in current-based recurrent IF networks (Zhang et al. 2014a; Zhang and Rangan 2015) and showed that by using a PEA formulation, we can design, from first principles, numerical algorithms that succeeded in capturing MFEs and provide a mathematical reduction that faithfully describes the many different, heterogeneous dynamical regimes of strongly coupled neuronal networks.

In the cortex, many experimental studies show the prevalence of high conductance states (Destexhe and Pare 1999; Destexhe et al. 2003; Shelley et al. 2002). High conductance states are often associated with high response variabilities and an enhancement in individual neuronal responses (Destexhe and Pare 1999; Destexhe et al. 2003). A high conductance necessarily leads to

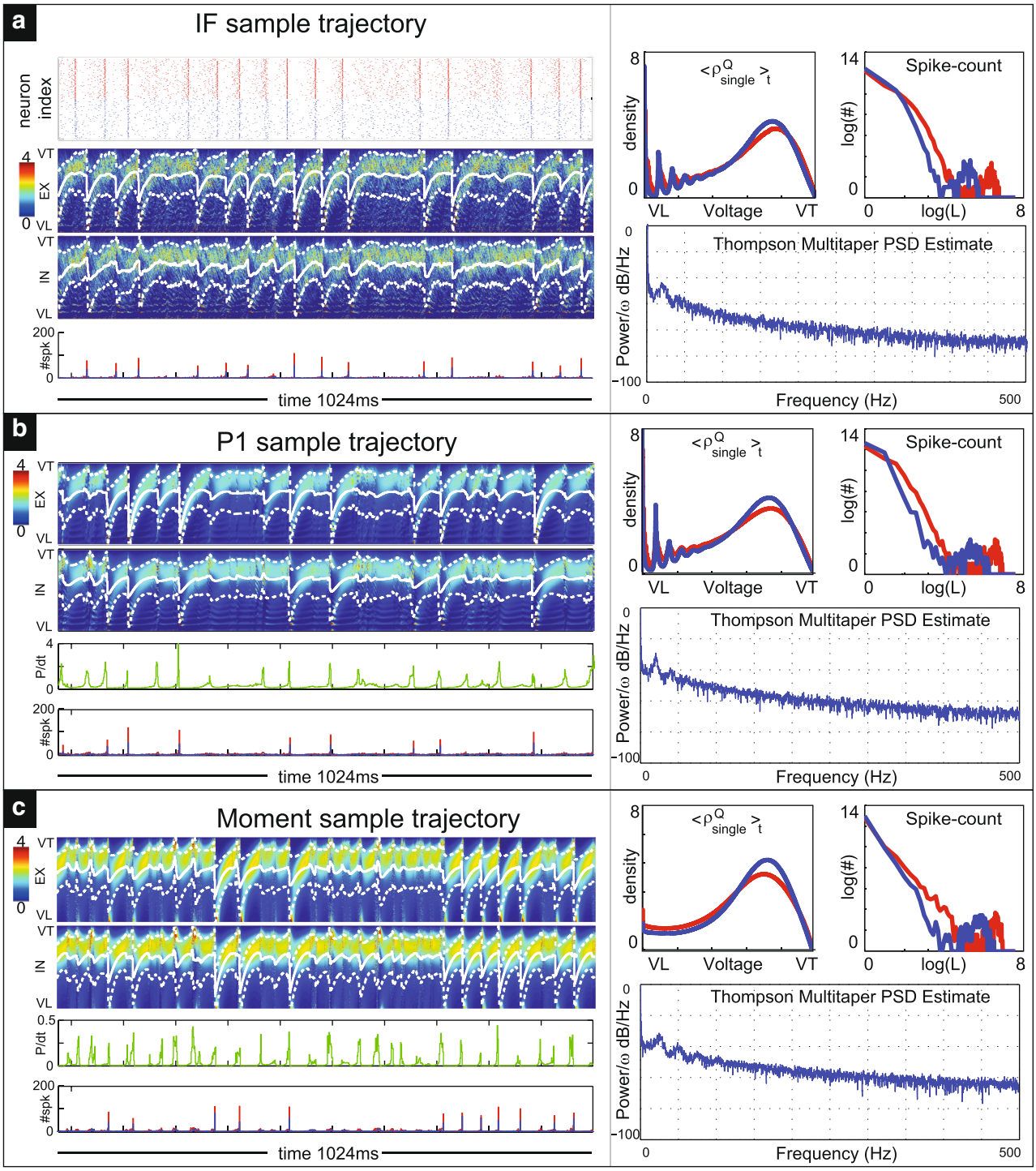

Fig. 5 A dynamical regime with many large MFEs. For this regime we have chosen $N_E = N_I = 128$, $S^{EE} = 0.00144$, $S^{II} = 0$, $S^{EI} = S^{IE} = 0.0006$, with $m_{net}^{EY} = 550Hz$, $m_{net}^{IY} = 540Hz$, and $S^{EY} = S^{IY} = 0.018$. Shown in panels **a**, **b** and **c** are examples of the IF, P1, and P2 trajectories in the stationary state. The left side of panel **a** shows an example of a raster plot (top), excitatory and inhibitory population voltage densities (middle), and spike counts (bottom). The voltage density traces show the time evolution of the voltage configuration $\varrho^Q(v,t)$ for the E- and I-cells in the network, with density magnitudes indicated in color (colorbar to the left). The mean voltage $\int v\varrho^Q dv$ is indicated by a solid white line, with $\pm$ 1 standard-deviation indicated by dashed white lines. The system spikes counts are collected over 1ms bins, and are separated into the E- (red) and I- (blue) populations. On the right side of panels **a,b,c**, we show the time-averaged voltage distributions $\int \varrho^Q dt$ averaged over the E- and I- cells in the network (upper left), as well as log-log plots of the system spike counts (upper right) and the PSD plots of the average system voltage (bottom). On the left of panels **b** and **c** we show the voltage density traces (top two) for the ρ^Q_{single}, as well as the corresponding time evolution of the MFE nucleation rate $P_{MFE}(t)/dt$ and system spike counts (bottom two)

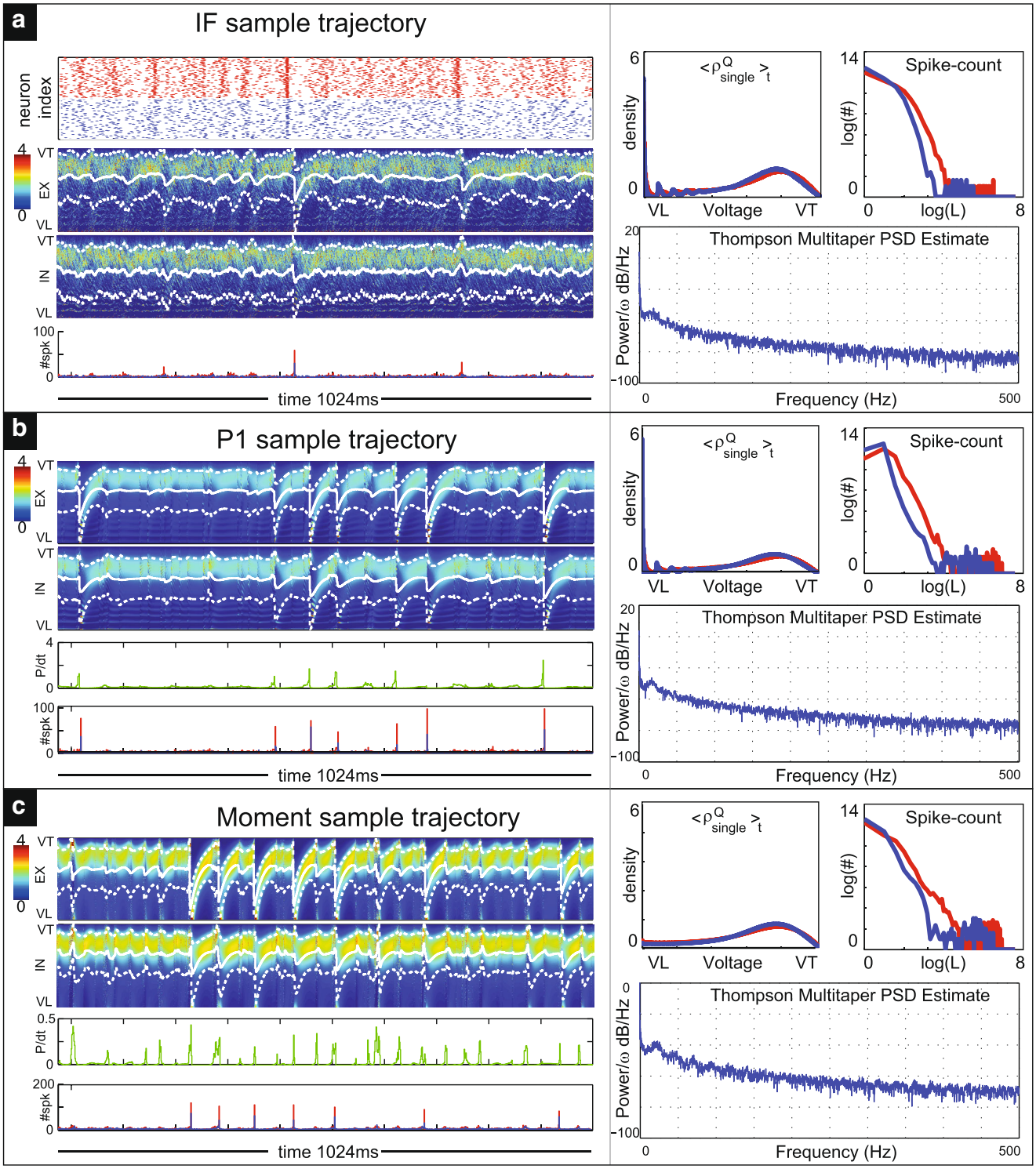

Fig. 6 A dynamic regime with small MFEs. The system and figure layout is identical to Fig. 5, with the exception that $S^{EE} = 0.00133$, $S^{II} = 0$, $S^{EI} = S^{IE} = 0.0006$

a reduced membrane time constant and implies network interactions on faster timescales. Modeling studies show that because of this reduced time constant, individual neurons can respond to faster frequency inputs and operate with increased temporal resolution (Destexhe et al. 2003; Shelley et al. 2002). Furthermore, our simulations reveal

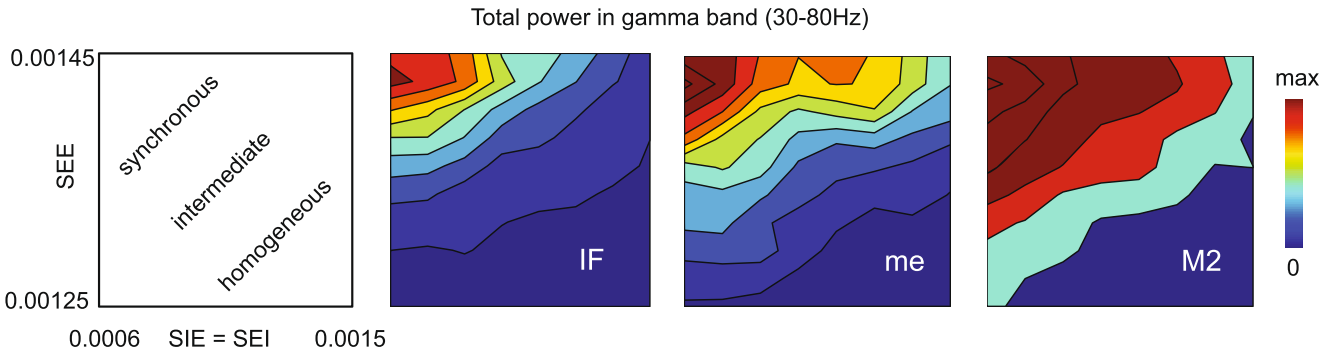

Fig. 7 A scan through parameter space. We fix the network parameters $N_E = N_I = 128$, $m_{net}^{EY} = 550Hz$, $m_{net}^{IY} = 540Hz$, and $S^{EY} = S^{IY} = 0.018$. We vary the coupling strengths S^{EE} and S^{EI} independently, setting $S^{IE} = S^{EI}$. When $S^{EE} \gg S^{EI}$ the dynamics are synchronous, when $S^{EE} \ll S^{EI}$ the dynamics are homogeneous, and when $S^{EE} \sim S^{EI}$ the dynamics are somewhere in between, as indicated in the leftmost panel. The other three panels show the γ-band power of the average system voltage in the stationary state as a function of coupling strength. The γ-band power is plotted relative to the maximum power observed across all simulations (see colorbar to the far right). Note that the coupling strength S^{EE} is varied over a small interval$[0.00125, 0.00144]$. That is to say, the variation of coupling strengths in L_2-norm is very small. Thus we can roughly compute the relative errors of parameter by $(0.0014 - 0.00135)/0.0014 \approx 3.57\%$, which represents the relative error between parameter for synchrony and the parameter for multiple firing events

that many statistical features of MFEs in conductance-based models differ significantly from current-based networks.

Therefore, we here extend the partitioned-ensemble average framework of Zhang et al. (2014a) and Zhang and Rangan (2015) to systematically coarse grain strongly coupled conductance-based IF neuronal networks. We first reduce the neuronal network to two 1D Master equations, and apply the PEA formulation to design a practical Algorithm-1 to deal with the dynamical regimes with frequent MFEs. Then, directly from the corresponding Fokker-Planck equations, we derive an augmented low-dimensional ODE system by introducing a hierarchy of voltage moments and a maximum entropy closure. Thus, in the end, we are able to reduce the spiking network dynamics to an Algorithm-2: (i) Evolving the moment equations with an optimization problem; (ii) At each time step, using the system's membrane potential distribution and synaptic strengths to calculate the probability of occurrence of an MFE; and (iii) When an MFE occurs, using the system's voltage distribution to sample the magnitude and depth of the MFE.

A Master equation approach in computational neuroscience was introduced by Ohira and Cowan (1993). More recent work can be found in El Boustani and Destexhe (2009), Buice et al. (2010), and Zerlaut et al. (2018), and references therein. In this work, the coarse-graining of network spikes to firing rates can be computed explicitly, whereas, in Zerlaut et al. (2018), the authors relied on fitting an effective threshold to model and coarse-grain the effect of the nonlinearities of a single neuron on its firing rate. However, by itself, the Master equation formalism cannot capture the transiently synchronous firing of many neurons, i.e., MFEs. Therefore, to capture the initiation and dynamics of these multiple-firing events, we had to introduce a hybrid formalism, the partitioned ensemble average, which, without the occurrence of MFEs, reduces back to the Master equation formalism (or the FP formalism, depending on your preferred coarse-graining model). In the PEA, the MFE is viewed as a special kind of transition and between these transitions, the usual ensemble average can be used.

Previously in Zhang and Rangan (2015), the derivation of the Master equation is conditioned on not generating MFEs. (We introduced a fraction of the time in order to keep the system from more firing events.) This intricate model leads to a complicated set of Master equations. In this paper, we relax this condition and use instead the methods of Cai et al. (2006) to derive a new Master equation and its corresponding FP equations. Furthermore, the exact steady-state solution of these FP equations can be computed and then used within a maximum entropy closure to reduce dramatically the mathematical description of the network dynamics to an augmented system of ODEs.

The methodology in this paper provides a conceptual framework to dimensionally reduce complex network spiking dynamics, and can qualitatively captured a vast range heterogeneous dynamics seen in neuronal networks. The method developed here treats explicitly the situation of instantaneous synapses - i.e., the synaptic time-scales τ_E and τ_I of the IF-network are both 0 (see the details in Appendix A). The reason for using instantaneous synapses is that, in this limit, individual MFEs are mathematically unambiguous. However, numerical studies (see, for instance, Rangan and Young 2013a, b) show that

the rapid dynamic transients much like MFEs are prevalent even when τ_Q are a few ms; consequently, even when τ_E and τ_I are increased to $\sim$ 2ms and $\sim$ 4 ms, our reduction can still faithfully capture many of the qualitative features of MFEs in strongly coupled conductance-based IF network dynamics.

Finally, we remark that we have detailed this methodology for a system with homogenous connectivities. Preliminary studies show that we can extend our framework to faithfully describe the emergent dynamics in networks with slowly varying spatial inhomogeneities (e.g., V1 orientation hypercolumns coupled by long-range excitatory connections; Shao et al, in preparation) and in capturing interneuronal correlations in predominantly feedforward, synfire chain-like, networks (see, for instance, Xiao et al. 2308). Future work will attempt to incorporate higher order motifs in the network connectivity (see also the discussions in Zhang et al. 2014a; Zhang and Rangan 2015). Higher order structural motifs are likely to substantially influence the types of correlations within complex networks, and consequently, activate other types of MFEs and spatio-temporal spiking patterns that may have important consequences for information processing and coding (Zhao et al. 2011; Hu et al. 2013).

Acknowledgments This work was partially supported by the Natural Science Foundation of China through grants 11771035 (J.Z.), 91430216 (J.Z.), U1530401 (J.Z.), 31771147 (Y.S., L.T.) and 91232715 (L.T.), by the Open Research Fund of the State Key Laboratory of Cognitive Neuroscience and Learning grant CNLZD1404 (Y.S., L.T.), and by the Beijing Municipal Science andTechnology Commission under contract Z151100000915070 (Y.S., L.T.).

Compliance with Ethical Standards

Conflict of interests The authors declare that they have no conflict of interest.

Appendix A: spike resolution

An important feature of the neuronal network we considered in this paper is that the synapses are instantaneous. In other words, the postsynaptic impulse response functions are taken to be δ-functions with no synaptic delay. This δ-function impulse response allows us to determine whether or not one neuron 'caused' another neuron to fire, i.e., the instantaneous synapses ensure that cascade-induced firing-events transpire instantaneously. Thus the feedforward inputs will not be confused with the network spikes. To clarify the dynamics that occurs whenever multiple neurons cross threshold simultaneously at time $t_{\rm spk}$, we consider our system to be a specific limit of the following fast conductance system

$$\begin{aligned}
\frac{dV_i^Q(t)}{dt} &= -g^E\left(V_i^Q - V_E\right) - g^I\left(V_i^Q - V_I\right), \qquad (34)\\
\tau_E\frac{dg^E(t)}{dt} &= -g^E + \sum_k S^{QE}\delta\left(t - t_{jk}^E\right),\\
\tau_I\frac{dg^I(t)}{dt} &= -g^I + \sum_k S^{QI}\delta\left(t - t_{jk}^I\right),
\end{aligned}$$

where the g^Q represent synaptic conductances, and the decay times $\tau_E \approx \tau_I \to 0$. Now at the time $t_{\rm spk}$, we freeze the macroscopic time t of the original system and create an "infinitesimal-time" system which evolves according to an infinitesimal time τ_Q. Since the MFE is initiated by one excitatory neuron firing before others, at $t_{\rm spk}$ the state-variables of the original system are given by

$$V_j^Q(t_{\rm spk}^-) \text{ for } j = 1, \cdots, N_Q \text{ with } V_1^E(t_{\rm spk}^-) \geq V_T. \qquad (35)$$

This infinitesimal-time system will use the infinitesimal time τ to describe the effects of the excitatory conductances in Eq. (36) by taking $\tau_E \approx \tau_I \to 0$. This is, at this macro-time $t_{\rm spk}$, we solve the dynamics of the infinitesimal system

$$\begin{aligned}
\frac{dV_i^Q(\tau)}{d\tau} &= -g^E\left(V_i^Q - V_E\right) - g^I\left(V_i^Q - V_I\right), \qquad (36)\\
\frac{dg^E(\tau)}{d\tau} &= -g^E + \sum_{j\neq i} S^{QE}\delta\left(\tau - \tau_j^E\right)\\
\frac{dg^I(\tau)}{d\tau} &= -g^I + \sum_{j\neq i} S^{QI}\delta\left(\tau - \tau_{jk}^I\right),
\end{aligned}$$

by fixing $\tau_E = \tau_I = 1$, letting the micro-time $\tau \to \infty$, and using the same conditions as Eq. (35). The spike-times τ_j^Q record the infinitesimal time at which neurons j fires. By denoting $r = g^I/g^E$ and $g(\tau) = g^E \cdot e^{-\tau}$, without ambiguity, we delete the subscript for a while, and rewrite the first equation in (36) as

$$\frac{dv}{d\tau} = -g(\tau)(1+r)(v - V_s),$$

where $V_s = (V_E + rV_I)/(1+r)$. Noteing that $\frac{dv}{d\tau} = \frac{dv}{dg}\frac{dg}{d\tau}$, we arrive at

$$\frac{dv}{dg} = (1+r)(v - V_s)$$

with the solution $v(\tau) = V_s + g^E(v_0 - V_s)e^{1+r}(1 - e^{-\tau})$. The voltage will evolve to a steady state of

$$\max(v) = \lim_{\tau\to\infty} v(\tau) = V_s + g^E(v_0 - V_s)e^{1+r}.$$

If $\max(v) \geq V_T$, the neuron will fire at time

$$\tau_j^Q = \tau' - \log\left[1 + \frac{1}{(1+r)g^E}\log\frac{V_T - V_s}{v_0 - V_s}\right],$$

where τ' is the time that the last previous neuron fires. By using this analytical formula, we can resolve the trajectory to machine precision during this infinitesimal time until the time $\tau = \min_{j,Q} \tau_j^Q$. Once a single neuron fires, it is clamped at V_R for a refractory period, and never fires again during this infinitesimal time. On the other hand, we can update the voltages of the other neurons that do not fire at this macro-time t_{spk}. After this infinitesimal time, we go back to the macro-time t to evolve the system. Thus we obtain a well-posed system of ODEs. One can see other similar implementation in Appendix B of Ref. Rangan and Young (2013a) and Appendix 12 of Ref. Zhang and Rangan (2015).

Appendix B: derivation of the Master equation $f_{B,single}$

In this section, the Master equation $\boldsymbol{f}_{B,single}$ is used to evolve the single-neuron distributions $\boldsymbol{\rho}_{single}(v,t) = (\rho^E_{single}, \rho^I_{single})$. Over the small voltage interval $[V_1, V_2]$, the total probability changes as a function of time. The difference from time t_1 to $t_1 + \Delta t$ is determined by the probability flux at the boundaries V_1 and V_2

$$\int_{v=V_1}^{v=V_2} \left[\rho^Q(v,t)\right]_{t=t_1}^{t=t_1+\Delta t} dv = f^Q_{B,single}\left(\rho^Q, v, t\right),$$

where $\boldsymbol{f}_{B,single} = \left(f^E_{B,single}, f^I_{B,single}\right)$ is given by

$$\begin{aligned} f^Q_{B,single}\left(\rho^Q, v, t\right) &= \int_{t_1}^{t_1+\Delta t} \left[g_L(v-V_L)\rho^Q(v,t)\right]_{v=V_1}^{v=V_2} dt \\ &+ \sum_{R\in\{E,I,Y\}} \int_{t_1}^{t_1+\Delta t} \int_{T(V_1,S^{QR})}^{T(V_2,S^{QR})} m^{QR}_{net}(t)\cdot\rho^Q(v,t)\,dvdt \\ &- \sum_{R\in\{E,I,Y\}} \int_{t_1}^{t_1+\Delta t} \int_{v=V_1}^{v=V_2} m^{QR}_{net}(t)\cdot\mathbf{1}_{[-\infty,T(V_T,S^{QR})]}(v)\cdot\rho^Q(v,t)\,dvdt \\ &- \int_{t_1}^{t_1+\Delta t} \int_{v=V_1}^{v=V_2} m^{QY}_{net}(t)\cdot\gamma^Q(t)\cdot\mathbf{1}_{[T(V_T,S^{QY}),V_T]}(v)\cdot\rho^Q(v,t)\,dvdt \\ &+ \mathbf{1}_{[V_1,V_2]}(V_L)\int_{t_1}^{t_1+\Delta t} \int_{T(V_T,S^{EY})}^{V_T} m^{QY}_{net}(t)\cdot\gamma^Q(t)\cdot\rho^Q(v,t)\,dvdt, \end{aligned} \tag{37}$$

where the fraction γ^I, and γ^E are used to condition $\boldsymbol{f}_{B,single}$ not to produce MFEs. The motivation to introduce γ^I and γ^E can be found in Zhang et al. (2014a). Generally, $\gamma^I \equiv 1$ and γ^E is given by the fraction of time that:

$$\gamma^E\left(t^+\right) = \left[\int_{-\infty}^{T(V_T,S^{EE})} \rho^E_{single}\left(v,t^-\right)dv\right]^{N_E-1} \times \left[\int_{-\infty}^{T(V_T,S^{IE})} \rho^I_{single}\left(v,t^-\right)dv\right]^{N_I}.$$

The network firing rates are given by:

$$\begin{aligned} m^{QE}_{net}\left(t^+\right) &= \left(N_Q - \delta_{QE}\right) m^E_{single}\left(t^-\right), \\ \text{and}\quad m^{QI}_{net}\left(t^+\right) &= \left(N_Q - \delta_{QI}\right) m^I_{single}\left(t^-\right), \end{aligned} \tag{38}$$

where the single-neuron firing rates $m^Q_{single}(t)$ represents the instantaneous firing rate of a single neuron in an ensemble driven by the various $m^{QR}_{net}(t)$, and is calculated by the flux of $\rho^Q(v,t)$ over the threshold point V_T at time t in form of

$$m^Q_{single}\left(t^-\right) = \int_{t_1}^{t_1+\Delta t} \int_{T(V_T,S^{EY})}^{V_T} m^{QY}_{net}(t)\cdot\gamma^Q(t)\cdot\rho^Q(v,t).$$

Appendix C: derivation of the standard Master equation

Here we derive the Master equation from system of conductance-based IF neuronal networks (1). We start by considering what can happen during a single time-interval of length Δt? The coarsest approximation involves choosing from amongst 5 possibilities: (i) the neuron starts out held in refractory and remains at V_L, (ii) the neuron starts out in (V_I, V_T) and decays naturally, (iii) the neuron starts out in (V_I, V_T) and gets a excitatory kick by the external input, or (iv,v) the neuron starts out in (V_I, V_T) and gets a kick of type-Q with synaptic coupling. The simplest possibility is (i), which can be treated by a straightforward computation. In possibility (ii), the pure decay case, v gets mapped to

$$R_L^{-1}(v, g_L\Delta t) = V_L + (v - V_L)\cdot e^{g_L\Delta t} = T_L(v, g_L\Delta t).$$

Thus, for a small dv, the distribution $\rho(v,t)\,dv$ within the interval $[v, v+dv]$ is replaced by

$$\rho\left(T_L(v,g_L\Delta t), t\right)\cdot T'_L(v,g_L\Delta t)\,dv = \rho\left(V_L + (v-V_L)\cdot e^{g_L\Delta t}, t\right)\cdot e^{g_L\Delta t}dv. \tag{39}$$

Now let us discuss possibilities (iii,iv,v) which correspond to getting a kick from the external input and other excitatory or inhibitory neurons in the network. For example, given a single kick of the external Poisson input, the distribution concentrated in the interval $[V_1, V_2]$gets mapped to the interval $\left[R\left(V_1, S^{QY}\right), R\left(V_2, S^{QY}\right)\right]$, and is mapped into by the interval $\left[T\left(V_1, S^{QY}\right), T\left(V_2, S^{QY}\right)\right]$. Thus, if $V_1 = v$, and $V_2 = v + dv$ for dv small, then $\rho(v)\,dv$ is replaced by $\rho\left(T\left(v, S^{QY}\right), t\right)\cdot T'\left(v, S^{QY}\right)dv$, implying that, for each voltage v, the distribution $\rho(v)$ is replaced by the distribution $\rho\left(T\left(v, S^{QY}\right), t\right)\cdot T'\left(v, S^{QY}\right) = \rho\left(V_E + (V - V_E)\cdot e^{S^{QY}}, t\right)\cdot e^{S^{QY}}$. Similarly, we have corresponding maps for excitatory and inhibitory network spikes.

Thus, combining these 5 possibilities, $\rho(v,t)$ evolves according to

$$\begin{aligned}\rho^Q(v,t+\Delta t) = &\left[1-(m_{net}^{QY}+N_E m^E+N_I m^I)\Delta t\right]\cdot\rho^Q\left(V_L+(V-V_L)\cdot e^{g_L\Delta t},t\right)\cdot e^{g_L\Delta t}\\ &+m_{net}^{QY}(t)\Delta t\cdot\rho^Q\left(V_E+(v-V_E)\cdot e^{S^{QY}},t\right)\cdot e^{S^{QY}}\\ &+N_E m^E(t)\Delta t\cdot\rho^Q\left(V_E+(v-V_E)\cdot e^{S^{QE}},t\right)\cdot e^{S^{QE}}\\ &+N_I m^I(t)\Delta t\cdot\rho^Q\left(V_I+(v-V_I)\cdot e^{S^{QI}},t\right)\cdot e^{S^{QI}}+\mathcal{S}^Q(t)\cdot\delta(V-V_R)\end{aligned}\tag{40}$$

with $Q\in\{E,I\}$. Taylor expanding,

$$\rho^Q\left(V_L+(V-V_L)\cdot e^{g_L\Delta t},t\right)\cdot e^{g_L\Delta t,t}=\rho^Q(v,t)+g_L\Delta t\partial_v[(v-V_L)\rho^Q(v,t)]+o(\Delta t).$$

Substituting the above into Eq. (40) and ignoring the terms of order $o(\Delta t)$ and higher, we arrive at

$$\begin{aligned}\rho^Q(v,t+\Delta t)-\rho^Q(v,t) = &\ g_L\Delta t\partial_v\left[(v-V_L)\rho^Q(v,t)\right]+m_{net}^{QY}(t)\Delta t\cdot\left[\rho^Q\left(T(v,S^{QY}),t\right)\cdot T'(v,S^{QY})-\rho^Q(v,t)\right]\\ &+N_E m^E(t)\Delta t\cdot\left[\rho^Q\left(T(v,S^{QE}),t\right)\cdot T'(v,S^{QE})-\rho^Q(v,t)\right]\\ &+N_I m^I(t)\Delta t\cdot\left[\rho^Q\left(T(v,S^{QI}),t\right)\cdot T'(v,S^{QI})-\rho^Q(v,t)\right]+\mathcal{S}^Q(t)\cdot\delta(V-V_R),\end{aligned}\tag{41}$$

where $\mathcal{S}^Q(t)$ is the flux across the threshold and is given by

$$\mathcal{S}^Q(t)=m_{net}^{QY}(t)\int_{T(V_T,S^{QY})}^{V_T}\rho^Q(v,t)dv+N_E m^E(t)\int_{T(V_T,S^{QE})}^{V_T}\rho^Q(v,t)dv.\tag{42}$$

Let $\Delta t\to 0$, we have the Master equation in the following form

$$\begin{aligned}\frac{d\rho^Q(v,t)}{dt} = &\ g_L\partial_v\left[(v-V_L)\rho^Q(v,t)\right]+m_{net}^{QY}(t)\cdot\left[\rho^Q\left(T(v,S^{QY}),t\right)\cdot T'(v,S^{QY})-\rho^Q(v,t)\right]\\ &+N_E m^E(t)\cdot\left[\rho^Q\left(T(v,S^{QE}),t\right)\cdot T'(v,S^{QE})-\rho^Q(v,t)\right]\\ &+N_I m^I(t)\cdot\left[\rho^Q\left(T(v,S^{QI}),t\right)\cdot T'(v,S^{QI})-\rho^Q(v,t)\right]+\mathcal{S}^Q(t)\cdot\delta(V-V_R).\end{aligned}\tag{43}$$

For a similar derivation of Eq. (43), see Nykamp (2000) and Cai et al. (2006).

Appendix D: derivation of Fokker-Planck equation

Similar to the reductions performed in Rangan and Cai (2006) and Helias et al. (2010), we take a single neuron driven only by the external Poisson input for example. More complicated case can be computed similarly. Let $s = e^{S^{QY}} - 1$, we can rewrite

$$T\left(v, S^{QY}\right) = v + s(v - V_E), \quad \text{and} \quad T'(v, S^{QY}) = 1 + s.$$

Ignoring the network synaptic connection for now, and considering only the external Poisson input, thus the Master Eq. (8) is given by

$$\partial_t \rho^Q(v,t) = g_L \partial_v \left[(v-V_L)\rho^Q(v,t)\right] + m_{net}^{QY}(t) \cdot \left[\rho^Q\left(v+(v-V_E)s, t\right)(1+s) - \rho^Q(v,t)\right]. \quad (44)$$

Taylor expanding and keeping the first order in s, we get

$$\rho^Q(v+(v-V_E)s) \approx \rho^Q(v) + (v-V_E)s\partial_v\rho^Q + \frac{(v-V_E)^2 s^2}{2}\partial_{vv}\rho^Q, \quad (45)$$

thus we can approximate (44) by

$$\begin{aligned}\partial_t \rho^Q(v,t) &= g_L \partial_v \left[(v-V_L)\rho^Q(v,t)\right] \\ &\quad + m_{net}^{QY}(t) \cdot \left[(v-V_E)s(1+s)\partial_v\rho^Q \right. \\ &\quad \left. + \frac{(v-V_E)^2 s^2(1+s)}{2}\partial_{vv}\rho^Q + s\rho^Q\right]. \quad (46)\end{aligned}$$

Noting the relationships

$$\begin{aligned}(v-V_E)s\partial_v\rho^Q &= \partial_v\left[s(v-V_E)\rho^Q\right] - s\rho^Q, \\ \frac{(v-V_E)^2 s^2}{2}\partial_{vv}\rho^Q &= \partial_v\left[\frac{(v-V_E)^2 s^2}{2}\partial_v\rho^Q\right] \\ &\quad - \partial_v\left[s^2(v-V_E)\rho^Q\right] + s^2\rho^Q,\end{aligned}$$

we have

$$\begin{aligned}&(v-V_E)s\partial_v\rho^Q + \frac{(v-V_E)^2 s^2}{2}\partial_{vv}\rho^Q \\ &= \partial_v\left[(s-s^2)(v-V_E)\rho^Q + \frac{(v-V_E)^2 s^2}{2}\partial_v\rho^Q\right] - (s-s^2)\rho^Q. \quad (47)\end{aligned}$$

Substituting (47) into (46), we arrive at the Fokker-Planck equation

$$\begin{aligned}\partial_t \rho^Q(v,t) &= \partial_v\{\left[g_L(v-V_L) + m_{net}^{QY}(t)(s-s^3)(v-V_E)\right]\rho^Q(v,t)\} \\ &\quad + \partial_v\{\frac{m_{net}^{QY}(t)(1+s)s^2(v-V_E)^2}{2}\partial_v\rho^Q\} + m_{net}^{QY}(t)s^3\rho^Q. \quad (48)\end{aligned}$$

We remark that the last term $m_{net}^{QY}(t)s^3\rho^Q$ in Eq. (48) has a small influence on the distribution when the parameter s is small. Hence, if we only keep the second order of s in the Taylor's expansion of Eq. (45), we can ignore this term in most practical analysis. Similarly, for the full IF network, we let $s = e^{S^{QY}} - 1$, $s_1 = e^{S^{QE}} - 1$, $s_2 = e^{S^{QI}} - 1$, and can approximate the Master Eq. (8) by a FP-type Eq. (9).

References

Abbott, L.F., & van Vreeswijk, C.A. (1993). Asynchronous states in networks of pulse-coupled neurons. *Physical Review E*, *48*, 1483–1488.

Anderson, J., Lampl, I., Reichova, I., Carandini, M., Ferster, D. (2000). Stimulus dependence of two-state fluctuations of membrane potential in cat visual cortex. *Nature Neuroscience*, *3*(6), 617–621.

Bak, P., Tang, C., Wiesenfeld, K. (1987). Self-organized criticality: an explanation of 1/f noise. *Physical Review Letters*, *59*(4), 381–384.

Battaglia, D., & Hansel, D. (2011). Synchronous chaos and broad band gamma rhythm in a minimal multi-layer model of primary visual cortex. *PLoS Computational Biology*, 7.

Buzsaki, G., & Wang, X.J. (2012). Mechanisms of gamma oscillations. *Annual Reviews in the Neurosciences*, *35*, 203–225.

Bornholdt, S., & Rohl, T. (2003). Self-organized critical neural networks. *Physical Review E*, *67*, 066118.

Bressloff, P.C. (2015). Path-integral methods for analyzing the effects of fluctuations in stochastic hybrid neural networks. *Journal of Mathematical Neuroscience*, *5*, 4.

Brunel, N. (2000). Dynamics of sparsely connected networks of excitatory and inhibitory spiking neurons. *The Journal of Comparative Neurology*, *8*, 183–208.

Brunel, N., & Hakim, V. (1999). Fast global oscillations in networks of integrate-and-fire neurons with low firing rates. *Neural Computation*, *11*, 1621–1671.

Bruzsaki, G., & Draguhn, A. (2004). Neuronal oscillations in cortical networks. *Science*, *304*, 1926–1929.

Buice, M.A., & Chow, C.C. (2007). Correlations, fluctuations, and stability of a finite-size network of coupled oscillators. *Physical Review E*, *76*, 031118.1-031118.25.

Buice, M.A., Cowan, J.D., Chow, C.C. (2010). Systematic fluctuation expansion for neural network activity equations. *Neural Computation*, *22*(2), 377–426.

Cai, D., Tao, L., Shelley, M., McLaughlin, D. (2004). An effective kinetic representation of fluctuation-driven neuronal networks with application to simple and complex cells in visual cortex. *Proceedings of the National Academy of Sciences of the United States of America*, *101*(20), 7757–7762.

Cai, D., Tao, L., Rangan, A., McLaughlin, D. (2006). Kinetic theory for neuronal network dynamics. *Communication in Mathematical Sciences*, *4*, 97–127.

Cardanobile, S., & Rotter, S. (2010). Multiplicatively interacting point processes and applications to neural modeling. *Journal of Computational Neuroscience*, *28*, 267–284.

Churchland, M.M. et al. (2010). Stimulus onset quenches neural variability: a widespread cortical phenomenon. *Nature Neuroscience*, *13*, 3:369–378.

Csicsvari, J., Hirase, H., Mamiya, A., Buzsaki, G. (2000). Ensemble patterns of hippocampal ca3-ca1 neurons during sharp wave-associated population events. *Neuron*, *28*, 585–594.

Destexhe, A., & Pare, D. (1999). Impact of network activity on the integrative properties of neocortical pyramidal neurons *in vivo*. *Journal of Neurophysiology*, *81*, 1531–1547.

Destexhe, A., Rudolph, M., Pare, D. (2003). The high-conductance state of neocortical neurons *in vivo*. *Nature Reviews. Neuroscience*, *4*, 739–751.

Dehghani, N., Hatsopoulos, N.G., Haga, N.G., Parker, R.A., Greger, B., Halgren, E., Cash, S.S., Destexhe, A. (2012). Avalanche analysis from multi-electrode ensemble recordings in cat, monkey and human cerebral cortex during wakefulness and sleep. *Frontiers in Physiology*, 3.

DeVille, L., & Zheng, Y. (2014). Synchrony and periodicity in excitable neural networks with multiple subpopulations. *SIAM Journal on Applied Dynamical Systems*, *13*(3), 1060–1081.

El Boustani, S., & Destexhe, A. (2009). A master equation formalism for macroscopic modeling of asynchronous irregular activity states. *Neural Computation*, *21*(1), 46–100.

Fourcaud, N., & Brunel, N. (2002). Dynamics of the firing probability of noisy integrate-and-fire neurons. *Neural Computation*, *14*, 2057–2110.

Fries, P. (2009). Neuronal gamma-band synchronization as a fundamental process in cortical computation. *Annual Review of Neuroscience*, *32*, 209–24.

Grill-Spector, K., & Weiner, K. (2014). The functional architecture of the ventral temporal cortex and its role in categorization. *Nature Reviews in the Neurosciences*, *15*, 536–548.

Hahn, G., Petermann, T., Havenith, M.N., Yu, S., Singer, W., Plenz, D., Nikolic, D. (2010). Neuronal avalanches in spontaneous activity *in vivo*. *Journal of Neurophysiology*, *104*, 3313–3322.

Hansel, D., & Sompolinsky, H. (1996). Chaos and synchrony in a model of a hypercolumn in visual cortex. *Journal of Computational Neuroscience*, *3*, 7–34.

Hatsopoulos, N.G., Ojakangas, C.L., Paniniski, L., Donoghue, J.P. (1998). Information about movement direction obtained from synchronous activity of motor cortical neurons. *Proceedings of the National Academy of Sciences*, *95*, 15706–15711.

Helias, M., Deger, M., Rotter, S., Diesmann, M. (2010). Instantaneous nonlinear processing by pulse-coupled threshold units. *PLoS Computational Biology*, *6*(9), e1000929.

Hertz, A.V.M., & Hopfield, J.J. (1995). Earthquake cycles and neural reverberations: collective oscillations in systems with pulse-coupled threshold elements. *Physical Review Letters*, *75*(6), 1222–1225.

Hu, Y., Trousdale, J., Josic, K., Shea-Brown, E. (2013). Motif statistics and spike correlations in neuronal networks. *Journal of Statistical Mechanics*, *P03012*, 1–51.

Kenet, T., Bibitchkov, D., Tsodyks, M., Grinvald, A., Arieli, A. (2003). Spontaneously emerging cortical representations of visual attributes. *Nature*, *425*, 954–956.

Knight, B. (1972). The relationship between the firing rate of a single neuron and the level of activity in a population of neurons. *The Journal of General Physiology*, *59*, 734.

Koch, C. (1999). *Biophysics of computation*. Oxford: Oxford University Press.

Kohn, A., & Smith, M.A. (2005). Stimulus dependence of neuronal correlation in primary visual cortex of the macaque. *Journal of Neuroscience*, *25*, 3661–73.

Kriener, B., Tetzlaff, T., Aertsen, A., Diesmann, M., Rotter, S. (2008). Correlatilons and population dynamics in cortical networks. *Neural Computation*, *20*, 2185–2226.

Ledoux, E., & Brunel, N. (2011). Dynamics of networks of excitatory and inhibitory neurons in response to time-dependent inputs. *Frontiers in Computational Neuroscience*, *5*, 25,1–17.

Leinekugel, X., Khazipov, R., Cannon, R., Hirase, H., Ben-Ari, Y., Buzsaki, G. (2002). Correlated bursts of activity in the neonatal hippocampus *in vivo*. *Science*, *296*, 2049–2052.

Litwin-Kumar, A., & Doiron, B. (2012). Slow dynamics and high variability in balanced cortical networks with clustered connections. *Nature Neuroscience*, *15*(11), 1498–1505.

Mazzoni, A., Broccard, F.D., Garcia-Perez, E., Bonifazi, P., Ruaro, M.E., Torre, V. (2007). On the dynamics of the spontaneous activity in neuronal networks. *PloS One*, *5*, e439.

Nykamp, D. (2000). A population density approach that facilitates large scale modeling of neural networks: analysis and application to orientation tuning. *Journal of Computational Neuroscience*, *8*, 19–50.

Newhall, K.A., Kovačič, G., Kramer, P.R., et al (2010). Cascade-induced synchrony in stochastically driven neuronal networks. *Physical Review E*, *82*(1), 041903.

Ohira, T., & Cowan, J.D. (1993). Master-equation approach to stochastic neurodynamics. *Physical Review. E, Statistical Physics, Plasmas, Fluids, and Related Interdisciplinary Topics*, *48*(3), 2259–2266.

Omurtag, A., Kaplan, E., Knight, B., Sirovich, L. (2000). A population approach to cortical dynamics with an application to orientation tuning. *Network: Computation in Neural Systems*, *11*(4), 247–260.

Ostojic, S., & Brunel, N. (2011). From spiking neuron models to linear-nonlinear models. *PLoS Computational Biology*, *7*, 1:e1001056.

Percival, D.B., & Walden, A.T. (1993). *Spectral analysis for physical applications*. Cambridge: Cambridge University Press.

Petermann, T., Thiagarajan, T.C., Lebedev, M.A., Nicolelis, M.A.L., Chailvo, D.R., Plenz, D. (2009). Spontaneous cortical activity in awake monkeys composed of neuronal avalanches. *Proceedings of the National Academy of Sciences*, *106*, 37:15921–15926.

Plenz, D., Stewart, C.V., Shew, W., Yang, H., Klaus, A., Bellay, T. (2011). Multi-electrode array recordings of neuronal avalanches in organotypic cultures. *Journal of Visualized Experiments*, *54*, 2949.

Poil, S.S., Hardstone, R., Mansvelder, H.D., Linkenkaer-Hansen, K. (2012). Critical-state dynamics of avalanches and oscillations jointly emerge from balanced excitation/inhibition in neuronal networks. *The Journal of Neuroscience*, *33*, 9817–9823.

Rangan, A.V. (2009). Diagrammatic expansion of pulse-coupled network dynamics. *Physical Reviews Letters*, *102*, 158101.

Rangan, A.V., & Cai, D. (2006). Maximum-entropy closures for kinetic theories of neuronal network dynamics. *Physical Review Letters*, *96*, 178101.

Rangan, A.V., & Young, L.S. (2013a). Dynamics of spiking neurons: between homogeneity and synchrony. *Journal of Computational Neuroscience*, *34*(3), 433–460.

Rangan, A.V., & Young, L.S. (2013b). Emergent dynamics in a model of visual cortex. *Journal of Computational Neuroscience*, *35*(2), 155–167.

Richardson, M.J. (1918). Effects of synaptic conductance on the voltage distribution and firing rate of spiking neurons. *Physical Review E*, *69*(05), 2004.

Robert, P., & Touboul, J. (2016). On the dynamics of random networks. *Journal of Statistical Physics*, *165*, 545–584.

Roopum, A.K., Kramer, M.A., Carracedo, L.M., Kaiser, M., Davies, C.H., Traub, R.D., Kopell, N.J., Whittington, M.A. (2008). Temporal interactions between cortical rhythms. *Frontiers in Neuroscience*, *2*, 145–154.

Roxin, A., Brunel, N., Hansel, D., Mongillo, G., Vreeswijk, C.V. (2011). On the distribution of firing rates in networks of cortical neurons. *The Journal of Neuroscience*, *31*(45), 16217–16226.

Sakata, S., & Harris, K.D. (2009). Laminar structure of spontaneous and sensory-evoked population activity in auditory cortex. *Neuron*, *12*(3), 404–418.

Samonds, J.M., Zhou, Z., Bernard, M.R., Bonds, A.B. (2005). Synchronous activity in cat visual cortex encodes collinear and cocircular contours. *Journal of Neurophysiology*, *95*, 4:2602–2616.

Seejnowski, T.J., & Paulsen, O. (2006). Network oscillations: emerging computational principles. *The Journal of Neuroscience*, *26*, 1673–1676.

Singer, W. (1999). Neuronal synchrony: a versatile code for the definition of relations? *Neuron*, *24*, 49–65.

Sirovich, L., Omurtag, A., Knight, B. (2000). Dynamics of neuronal populations; the equilibrium solution. *SIAM Journal on Applied Mathematics*, *60*, 2009–2028.

Shelley, M., McLaughlin, D., Shapley, R., Wielaard, J. (2002). States of high conductance in a large-scale model of the visual cortex. *Journal of Computational Neuroscience*, *13*, 93–109.

Shew, S., Yang, H., Yu, S., Roy, R., Plenz, D. (2011). Information capacity and transmission are maximized in balanced cortical networks with neuronal avalanches. *The Journal of Neuroscience*, *31*, 55–63.

Stern, E.A., Kincaid, A.E., Wilson, C.J. (1997). Spontaneous subthreshold membrane potential fluctuations and action potential variability of rat corticostriatal and striatal neurons *in vivo*. *Journal of Neurophysiology*, *77*, 1697–1715.

Storch, H., & Zwiers, F.W. (2001). *Statistical analysis in climate research*. Cambridge University Press.

Touboul, J. (2014). Propagation of chaos in neural fields. *Annals of Applied Probability*, *24*, 1298–1328.

Traub, R.D., Jeffreys, J., Whittington, M. (1999). *Fast oscillations in cortical circuits*. Cambridge: MIT Press.

Vogels, T.P., & Abbott, L.F. (2005). Signal propagation and logic gating in networks of integrate-and-fire neurons. *The Journal of Neuroscience*, *25*, 10786–95.

Werner, G. (2007). Metastability, criticality and phase transitions in brain and its models. *BioSystems*, *90*, 496–508.

Xiao, Z.C., Zhang, J.W., Sornborger, A.T., Tao, L. (2308). Cusps enable line attractors for neural computation. *Physical Review E*, *96*(05), 2017.

Yu, Y., & Ferster, D. (2010). Membrane potential synchrony in primary visual cortex during sensory stimulation. *Neuron*, *68*, 1187–1201.

Yu, S., Yang, H., Nakahara, H., Santos, G.S., Nikolic, D., Plenz, D. (2011). Higher-order interactions characterized in cortical activity. *The Journal of Neuroscience*, *31*, 17514–17526.

Zerlaut, Y., Chemla, S., Chavane, F., Destexhe, A. (2018). Modeling mesoscopic cortical dynamics using a mean-field model of conductance-based networks of adaptive exponential integrate-and-fire neurons. *Journal of Computational Neuroscience*, *44*, 45–61.

Zhang, J., & Rangan, A.V. (2015). A reduction for spiking integrate-and-fire network dynamics ranging from homogeneity to synchrony. *Journal of Computational Neuroscience*, *38*(2), 355–404.

Zhang, J.W., Zhou, D., Cai, D., Rangan, A.V. (2014a). A coarse-grained framework for spiking neuronal networks: between homogeneity and synchrony. *Journal of Computational Neuroscience*, *37*(1), 81–104.

Zhang, J.W., Newhall, K., Zhou, D., Rangan, A.V. (2014b). Distribution of correlated spiking events in a population-based approach for integrate-and-fire networks. *Journal of Computational Neuroscience*, *36*(2), 279–295.

Zhao, L.Q., Beverlin, B., Netoff, T., Nykamp, D.Q. (2011). Synchronization from second order network connectivity statistics. *Frontiers in Computational Neuroscience, 5*(28).

Affiliations

Jiwei Zhang[1,2] · Yuxiu Shao[3,4] · Aaditya V. Rangan[5] · Louis Tao[3,4]

Jiwei Zhang
jiweizhang@whu.edu.cn

Yuxiu Shao
shaoyx@mail.cbi.pku.edu.cn

Aaditya V. Rangan
rangan@cims.nyu.edu

1 School of Mathematics and Statistics, Wuhan University, Wuhan 430072, China

2 Hubei Key Laboratory of Computational Science, Wuhan University, Wuhan 430072, China

3 Center for Bioinformatics, National Laboratory of Protein Engineering and Plant Genetic Engineering, School of Life Sciences, Peking University, Beijing, 100871, China

4 Center for Quantitative Biology, Peking University, Beijing, 100871, China

5 Courant Institute of Mathematical Sciences, New York University, New York, NY, USA